NAR Breakthrough Article

RNA-regulatory exosome complex confers cellular survival to promote erythropoiesis

Charu Mehta[1,2], Isabela Fraga de Andrade[1,2], Daniel R. Matson[1,2], Colin N. Dewey [3] and Emery H. Bresnick [1,2,*]

[1]Department of Cell and Regenerative Biology, Wisconsin Blood Cancer Research Institute, University of Wisconsin School of Medicine and Public Health, Madison, WI 53705, USA, [2]Carbone Cancer Center, University of Wisconsin School of Medicine and Public Health, Madison, WI 53705, USA and [3]Department of Biostatistics and Medical Informatics, University of Wisconsin, Madison, WI 53705, USA

ABSTRACT

Cellular differentiation requires vast remodeling of transcriptomes, and therefore machinery mediating remodeling controls differentiation. Relative to transcriptional mechanisms governing differentiation, post-transcriptional processes are less well understood. As an important post-transcriptional determinant of transcriptomes, the RNA exosome complex (EC) mediates processing and/or degradation of select RNAs. During erythropoiesis, the erythroid transcription factor GATA1 represses EC subunit genes. Depleting EC structural subunits prior to GATA1-mediated repression is deleterious to erythroid progenitor cells. To assess the importance of the EC catalytic subunits Dis3 and Exosc10 in this dynamic process, we asked if these subunits function non-redundantly to control erythropoiesis. Dis3 or Exosc10 depletion in primary murine hematopoietic progenitor cells reduced erythroid progenitors and their progeny, while sparing myeloid cells. Dis3 loss severely compromised erythroid progenitor and erythroblast survival, rendered erythroblasts hypersensitive to apoptosis-inducing stimuli and induced γ-H2AX, indicative of DNA double-stranded breaks. Dis3 loss-of-function phenotypes were more severe than those caused by Exosc10 depletion. We innovated a genetic rescue system to compare human Dis3 with multiple myeloma-associated Dis3 mutants S447R and R750K, and only wild type Dis3 was competent to rescue progenitors. Thus, Dis3 establishes a disease mutation-sensitive, cell type-specific survival mechanism to enable a differentiation program.

INTRODUCTION

Beyond transcription, establishing and maintaining physiological programs of gene expression require post-transcriptional control of RNA processing, splicing and degradation, which collectively establish functional transcriptomes and proteomes. Considering the vast cellular remodeling required for stem/progenitor cell differentiation, it is instructive to consider the role of RNA-regulatory machinery as instigators or promoters of differentiation. Post-transcriptional mechanisms might be particularly critical for regulating transcriptomes during differentiation as large sectors of the genomes are destined to become transcriptionally repressed. Since lineage-specific gene priming in multipotent cells generates RNAs prior to protein requirements, presumably, post-transcriptional mechanisms prevent precocious translation and proteome remodeling. Independent of transcriptome regulation in differentiated cells and lineage-priming, integrating post-transcriptional with transcriptional regulation elevates opportunities to dynamically control transcripts and associated cellular functions.

The RNA exosome complex (EC) selectively degrades or processes multiple classes of RNAs (1–6). The 11-subunit nuclear EC complex contains Dis3 and Exosc10 catalytic subunits and a nine-subunit structural core (7). Within this core, Exosc1, Exosc2 and Exosc3 form a trimeric cap. S1/KH domains of the cap proteins create a channel to permit RNA entrance into the catalytic core. Ex-

osc4, Exosc5, Exosc6, Exosc7, Exosc8 and Exosc9 assemble a ring-like hexameric structure containing PH domains that promote RNA binding (8–10) (Figure 1A). Context-dependent cofactors, e.g. UPF factors, TRAMP, NEXT and PAXT complexes, also mediate RNA binding (11–13).

Dis3 and Exosc10, which endow the EC with catalytic activity, are processive and distributive 3′-5′ exoribonucleases, respectively; Dis3 also has endonuclease activity (1,14,15). Murine Dis3 shares amino acid sequence identity with human Dis3 (>90%) and yeast Rrp44 (43%). Dis3 contains a Pilus-forming N-terminus domain with endoribonuclease activity, two cold-shock domains (CSD1 and CSD2), a 3′-5′ ribonuclease B domain (RNB) and a C-terminal S1 domain (Figure 1A). Exosc10 contains a polycystin 2 N-terminal domain that binds Rrp47, a yeast RNA-binding EC cofactor, a DEDD-Y family 3′-5′ exoribonuclease domain, and helicase and RNase D carboxy-terminal domains (Figure 1A) (16,17). While the Dis3/Rrp44 structure resembles bacterial RNase II and RNase R, the Exosc10/Rrp6 exonuclease domain is homologous to RNase D (15,18). The yeast *Dis3* ortholog (*Rrp44*) is an essential gene (1,3). Human Dis3 partially rescues Rrp44 loss in yeast (7). Loss of the yeast *Exosc10* ortholog (*Rrp6*) yields defective growth at restrictive temperatures, while loss of other EC subunits is lethal at all temperatures; thus, *Rrp6* is non-essential in yeast (14,19). In HEK293 and HeLa cells, Dis3 is predominantly nuclear, whereas Exosc10 is enriched in the nucleolus (7,20).

Although the EC has not been studied extensively in mammalian systems, loss-of-function analyses have revealed critical roles in stem and progenitor cells and select differentiated cell types. Exosc9 regulates *GRHL3*, a transcription factor required for human epidermal progenitor cell differentiation (21). The EC also regulates AID activity in B-cells to enable generation of a diverse antibody repertoire. EC disruption upregulates lncRNAs and eRNAs in murine B-cells and maintains ES cell pluripotency (4,5). Rapid depletion of Dis3 or Exosc10 in HCT116 colon cancer cells abrogates colony formation, yet Dis3 depletion caused a greater accumulation of PROMPTs, eRNAs and premature cleavage and poly-adenylation (PCPA) products (6). The erythroid transcription factor GATA1, which is essential for erythropoiesis (22–24), and its cooperating transcription factor FOXO3 repress EC subunit genes during differentiation (12,25). Exosc8 or Exosc9 downregulation disrupts EC integrity, reduces BFU-E (Burst Forming Unit-Erythroid) and promotes differentiation in a mechanism involving reduced expression of the receptor tyrosine kinase c-Kit (26). We proposed that the EC controls erythropoiesis by balancing erythroid precursor expansion and differentiation. Our prior strategy disrupted the EC structural core, and the phenotypes might or might not predict those from impaired catalytic activity. As many unanswered questions exist about EC function in differentiation, and mechanisms underlying the EC requirement for erythroid progenitor cells are incompletely understood, we analyzed catalytic subunit functions and assessed if disrupting catalytic activity unveils unique mechanistic and/or biological insights.

MATERIALS AND METHODS

EC molecular structures

Protein structure coordinate files for the human EC (10) were downloaded from the Research Collaboratory for Structural Bioinformatics Protein Data Bank (www.RCSB.org, accession number 6D6Q). Images were generated using PyMOL (www.PyMOL.org, Schrödinger, New York, NY).

Mouse timed matings

E14.5 wild-type C57BL/6J embryos were obtained from timed matings. Pregnant females were euthanized with CO_2, and the uterus was removed into IMDM (Gibco) containing 10% FBS (Gemini). Fetal livers were harvested in IMDM containing 10% FBS. All mouse experiments were performed with the ethical approval of the AAALAC International (Association for the Assessment and Accreditation of Laboratory Animal Care) at UW-Madison.

Primary erythroid precursor cell isolation and culture

Hematopoietic progenitors were enriched from E14.5 fetal livers via negative enrichment with magnetic separation (27). Fetal liver cells were resuspended at 5×10^6 cells/ml in phosphate-buffered saline (PBS) containing 2% FBS, 2.5 mM ethylenediamine tetraacetic acid (EDTA) and 10 mM glucose. Biotinylated lineage-specific antibodies CD3e, CD11b, CD19, CD45R, GR-1 and CD71 at 3 µl/ml and biotinylated Ter119 at 5 µl/ml were added to the cells and incubated for 15 min on ice. Cells were washed by centrifugation for 5 min at 1200 rpm at 4°C and resuspended at 5×10^6 cells/ml in PBS containing 2% FBS, 2.5 mM EDTA and 10 mM glucose. Streptavidin beads were added at 75 µl/ml. After 15 min at 4°C, cells were resuspended to 2.5 ml and incubated for 5 min with a magnet. For erythroid and myeloid culture, cells were cultured in IMDM supplemented with 1% IL-3 containing conditioned medium and 1% conditioned medium from a Kit-ligand producing CHO cell line. For erythroid expansion culture, precursors were maintained at a density of $2.5–3.5 \times 10^5$ cells/ml in StemPro-34 (Gibco, 10639–011) supplemented with 10% nutrient supplement (Gibco, 10641-025), 2 mM L-glutamine (Cellgro), 1% penicillin–streptomycin (Cellgro, 30-002-CI), 100 µM monothioglycerol (Sigma), 1 µM dexamethasone (Sigma), 0.5 U/ml of erythropoietin and 1% conditioned medium from a Kit ligand-producing CHO cell line. All cells were grown in a humidified incubator at 37°C with 5% carbon dioxide. All percentages are v/v unless otherwise noted.

Flow cytometry

E14.5 fetal liver cells were dissociated and resuspended in PBS with 2% FBS and passed through 25 µm cell strainers to obtain single-cell suspensions prior to antibody staining. Erythroid and myeloid populations were analyzed using combinations of APC-Ter-119, PE Cy7-c-Kit (Biolegend, 105814), PE-CD71 (Biolegend, 113808), Mac1-APCe780 (47-0112-82) and/or Gr1-PE-Cy7 (Biolegend, 108416) at 4°C for 30 min. After staining, cells were washed once with
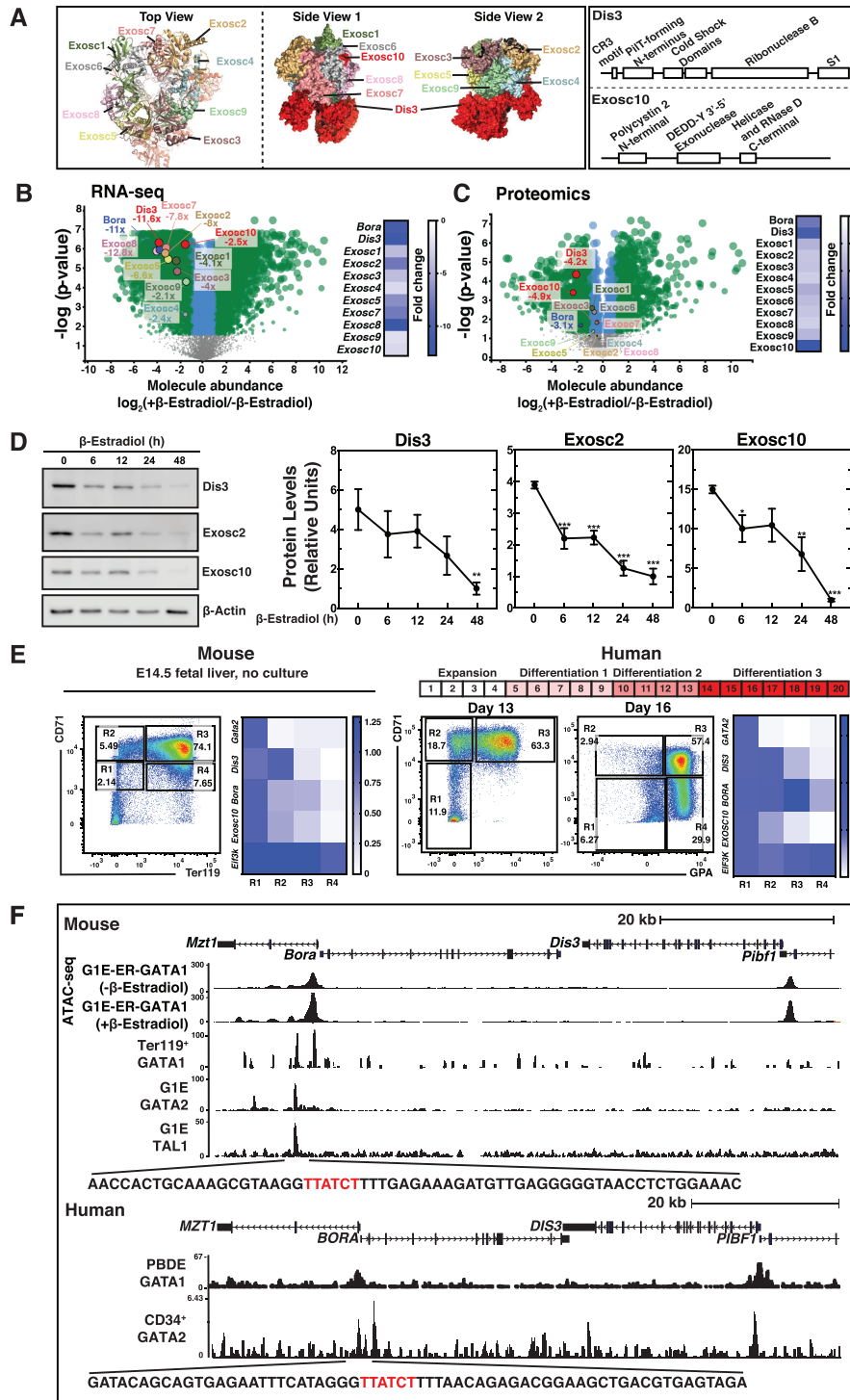
Figure 1. GATA1 downregulates EC catalytic subunits. (**A**) Left, EC crystal structure determined by electron microscopy ([10]). Exosc10 structure was partially resolved in this model; the image depicts only its EC-interacting region (red); right, domain organization of Dis3 and Exosc10, the EC catalytic subunits. (**B**) RNA-seq was conducted in G1E-ER-GATA1 cells before and after β-estradiol treatment, genes encoding EC subunits and Bora are highlighted with fold changes (dataset from: ([34])). (**C**) Proteomic analysis was conducted in G1E-ER-GATA1 cells before and after β-estradiol treatment. EC subunits and Bora are highlighted with fold changes (dataset from: ([33])). (**D**) Left, representative Western blots; right, quantitation of Dis3, Exosc2 and Exosc10 protein levels in G1E-ER-GATA1 cells. Values were normalized to β-actin. The data represent mean ± SEM ($n = 6$). (**E**) Left, representative flow plot of primary murine fetal liver cells sorted using CD71-Ter119 and heat map of RT-PCR analysis of *Gata2, Dis3, Bora, Exosc10* and *Eif3k* mRNA levels ($n = 5$), right, representative flow plot of primary human cells sorted using CD71-GPA and heat map of RT-PCR analysis of *GATA2, DIS3, BORA, EXOSC10* and *EIF3K* mRNA levels in peripheral blood-derived erythroblasts cultured in a 20-day differentiation system ($n = 5$). Values were normalized to 18S rRNA expression. (**F**) Chromatin state (ATAC-seq) in G1E-ER-GATA1 cells (dataset from: ([38])), GATA1 and GATA2 occupancy at *Dis3* and *Bora* loci in mouse and human cells ([39–41]). Statistically significant differences are indicated *$P < 0.05$, **$P < 0.01$, ***$P < 0.001$ using two-tailed unpaired Student's *t*-test.

2% FBS, 10 mM glucose and 2.5 mM EDTA in PBS. The cells were analyzed on an Attune™ NxT Flow Cytometer (Thermofisher Scientific) or collected on a FACSAria II cell sorter (BD Biosciences). To quantify apoptosis and CD71/Ter119 levels, the cells were washed in Annexin V Buffer (10 mM HEPES, 140 mM NaCl, 2.5 mM CaCl$_2$, pH 7.4) and stained with Annexin V-Pacific blue (ThermoFisher, A35122) (1:40) and DRAQ7 (Abcam, ab109202) (1:100) for 20 min in the dark at room temperature. After staining, cells were washed once in PBS containing 10% FBS or PBS containing 2% FBS, 10 mM glucose and 2.5 mM EDTA. The stained cells were analyzed on a Attune™ NxT Flow Cytometer flow cytometer (Thermofisher Scientific) or collected on a FACSAria II cell sorter (BD Bioscience). The data were analyzed using FlowJo v10.1 software (TreeStar).

Colony forming unit assays

For CFU assays, fetal liver cells sorted 20–24 h postinfection were plated in duplicate in Methocult M3434 complete media (StemCell Technologies) in 35 mm plate. CFU-Es were enumerated on day 3, and BFU-Es and CFU-GMs were enumerated on day 8 in a single-blinded manner.

Immunofluorescence

Cells were collected on poly-lysine coated slides and fixed with 3.7% paraformaldehyde in PBS for 10 min at room temperature. Slides were washed with PBS and were permeabilized with 0.2% Triton X-100 for 10 min at room temperature. Washed slides were blocked with 3% BSA in 0.1% Tween 20 in PBS for 1 h at 37°C and incubated with anti-HA (Covance HA.11, MMS-101P) or anti-Ser139-γ-H2AX (Millipore Sigma, 05-636) in 3% BSA at 4°C overnight. After washing, slides were incubated with secondary antibody for 1 h at 37°C. Slides were washed and mounted using Vectashield mounting medium with DAPI (Vector Laboratories). Images were acquired with a Nikon A1R-S confocal microscope. γ-H2AX signals were quantified as integrated density using FIJI (28) in a double-blinded manner.

Gene expression analysis

Total RNA was purified from cells using TRIzol (Invitrogen). cDNA was synthesized by Moloney murine leukemia virus reverse transcription (M-MLV RT). Real-time PCR was conducted with SYBR green master mix using a Viia7 instrument (Applied Biosystems). Control reactions lacking M-MLV RT yielded little to no signal. Relative expression was determined from a standard curve of serial dilutions of cDNA samples, and values were normalized to 18S RNA expression and to *Eif2s1* RNA for rRNA intermediate precursor analysis.

Protein analysis

Equal numbers of sorted cells harvested and boiled for 10 min in sodium dodecyl sulfate (SDS) lysis buffer (50 mM Tris (pH 6.8), 2% β-mercaptoethanol, 2% SDS,

0.1% bromophenol blue, 10% glycerol) were resolved on 7.5 or 10% SDS-polyacrylamide gels and analyzed by semi-quantitative Western blotting with ECL Plus (Pierce) and West Femto (Pierce) with rabbit polyclonal anti-mouse Dis3 (Protein Tech, 14689-1-AP) or anti-mouse Exosc10 (Santa Cruz, SC-374595), anti-mouse Exosc2 (Abcam #ab156698), HA (Covance HA.11, MMS-101P), anti-mouse α-tubulin (Cell Signaling Technology, #3873) or anti-mouse β-actin (Cell Signaling Technology, #3700).

Statistics

For cell, cell colony, or mRNA quantitation, the results are presented as box-and-whisker plots, with the box depicting the 25–75th percentiles of data, the line representing the median, and the whiskers ranging from minimum to maximum values. Determination of significance was conducted using the two-tailed unpaired Student's *t* test. A *P* value less than 0.05 was considered significant. For statistical analysis of integrated γ-H2AX signal density, statistical significance was calculated using Kruskal-Wallis test using Prism by Graphpad software. A *P* value <0.05 was considered significant.

RNA-seq analysis

GFP$^+$ erythroid precursors (CD71^{int}Ter119$^-$) and proerythroblasts (CD71$^{int/+}$Ter119$^-$) were purified from firefly luciferase, Dis3 or Exosc10 shRNA-expressing fetal liver cells. RNA-seq was conducted in quadruplicate with RNA isolated from cells sorted 2 days after erythroid expansion culture. rRNA-depleted total RNA was used to generate libraries with the Takara Stranded RNA v2 Pico library kit.

RNA-seq data were generated with an Illumina NovaSeq 6000 sequencer as 151 bp paired-end reads. Gene and isoform-level read counts were estimated using RSEM v1.3.0 (29) with mouse genome assembly version mm10 and GENCODE gene annotation version M24. Via the parameters '–star –star-output-genome-bam', RSEM used STAR v2.5.3a (30) to align the reads to the genome. RSEM was also passed the parameters '–forward-prob 0 –paired-end' to take into account the paired-end and strand-specific nature of the data.

Examination of the alignments to the genome revealed that the samples varied in terms of 'background' read coverage, presumably due to DNA contamination. This variation was not associated with the treatment groups. We quantified DNA contamination by computing the mean read coverage (second read only) within 1000 randomly sampled intergenic intervals each of length 10 kb. Intergenic intervals were required to be at least 5 kb from an annotated transcript.

Differential expression analyses were conducted with the DESeq2 v1.26.0 R package (31). For gene-level analyses, only genes with mean coverage >3 FPKM in at least one treatment group were considered for analysis. To control for variable DNA contamination, read counts were modeled with a generalized linear model with a categorical factor for treatment group (shDis3, shExosc10 or shLuc) and a continuous factor defined as the logarithm of each sample's intergenic read coverage estimated as described above. Differentially expressed genes were taken to be those with

an adjusted *P*-value <0.05 for each pairwise comparison of treatment groups.

For antisense transcription analysis, we calculated read coverage within the initial exon and 2 kb antisense upstream region on the opposite strand of each annotated transcript. Only the second read of each pair was considered for this analysis and a read was counted for a region if it uniquely aligned to the genome, overlapped any portion of the region, and mapped to the same strand as the region. These calculations were performed with the summarizeOverlaps function of the GenomicAlignments R package (32). We removed from consideration any transcript in which the antisense upstream region overlapped with an annotated exon on the same strand. We then selected the transcript from each gene with the highest median read coverage amongst all transcripts annotated for that gene. Finally, we removed from consideration any transcript that had zero-read coverage at its initial exon in one or more samples, to ensure that we restricted analysis to transcripts that were consistently transcribed. Differential expression of the resulting set of initial exons and antisense upstream regions was conducted in a combined analysis using DESeq2 with the same model as for the gene-level analysis.

RESULTS

EC dismantling during erythroid differentiation

GATA1 represses EC subunit gene transcription as erythroid precursor cells differentiate into erythrocytes, and the repression promotes a transition from precursor proliferation to differentiation (25,26). Our prior multi-omic (RNA-seq/quantitative proteomic) analysis established GATA1-regulated mRNAs and proteins during differentiation of the GATA1-null mouse proerythroblast cell line G1E-ER-GATA1 (33,34). These cells stably express a conditionally-active ER-GATA1 allele, and their differentiation recapitulates a normal window of erythropoiesis (35,36). RNA-seq revealed downregulation of transcripts encoding multiple EC subunits (from 13-fold for *Exosc8* to 2.1-fold for *Exosc9* mRNAs) upon differentiation (Figure 1B). As EC protein expression had not been analyzed during differentiation, we mined the proteomic data, which revealed reduced EC subunit levels, with the catalytic subunits Exosc10 (4.9-fold) and Dis3 (4.2-fold) decreasing to the greatest extent (Figure 1C). Semi-quantitative Western blotting validated the EC catalytic subunit decreases in G1E-ER-GATA1 cells treated with β-estradiol for up to 48 hours. At 48 hours, Dis3, Exosc2 and Exosc10 proteins decreased 4.4-, 3.9- and 15-fold, respectively (Figure 1D). *Dis3* and *Exosc10* expression were reduced upon differentiation of primary mouse and human erythroid cells, whereas murine *Eif3k* and human *EIF3K* expression were constant (Figure 1E). Thus, reduced EC catalytic subunit expression is a conserved hallmark of erythroid differentiation. To gain mechanistic insights, we analyzed genes flanking *Dis3* and *Exosc10*. The Dis3-neighboring gene *Bora*, encoding an activator of the cell cycle regulator Aurora-A kinase (37), was also downregulated.

The transcription factor GATA1 activates and represses transcription to establish networks that enable erythroid progenitor survival and differentiation into erythrocytes

(24). We asked if GATA1 occupies the genetic loci encoding EC catalytic subunits. We analyzed ATAC-seq and ChIP-seq data from diverse erythroid systems: (i) undifferentiated and β-estradiol-induced (differentiated) G1E-ER-GATA1 cells (38); (ii) GATA1-expressing primary Ter119+ murine erythroblasts (39) (iii) G1E cells lacking ER-GATA1 and expressing endogenous GATA2 (39), which maintains precursors prior to GATA1 expression; (iv) GATA1-expressing peripheral blood-derived human erythroblasts (PBDE) (40); and (v) GATA2-expressing human CD34+ cells (41) (Figure 1F, Supplementary Figure S1). In the murine cells, GATA1 occupied a region ∼1.3 kb upstream of *Bora,* within an intron of the neighboring gene *Mzt1,* corresponding to an open chromatin region in G1E-ER-GATA1 cells (38). While ER-GATA1 did not regulate *Mzt1* expression in G1E-ER-GATA1 cells, ER-GATA1 downregulated *Bora* mRNA (11-fold) and protein (3.1-fold), resembling *Dis3* (Figure 1B, C). GATA1 occupied the cognate human site containing a conserved WGATAR motif (AGATAA). In G1E cells, GATA2 occupied this site, as well as TAL1, which often co-localizes with GATA2 on chromatin (39,41–43). As GATA1 occupancy correlated with repression of the adjacent *Dis3* and *Bora* genes, this co-regulation might reflect a functional link. Though Bora has not been studied in hematopoiesis, Aurora-A is essential for hematopoiesis, and an Aurora-A inhibitor attenuates primary myelofibrosis phenotypes (44). GATA1 also occupies a site downstream of the murine *Exosc10* locus. In human peripheral blood-derived erythroblasts, GATA1 occupies a site upstream of *EXOSC10* (Supplementary Figure S1).

We tested whether Dis3 and Bora are GATA1-regulated determinants of hematopoietic progenitor differentiation. In lineage-depleted (Lin−) fetal liver hematopoietic progenitors, shRNA-expressing retroviruses downregulated *Bora* and *Dis3* 60% and 75%, respectively (Figure 2A). Twenty four hours post-infection, 5000 GFP+ cells were plated in methylcellulose to quantify erythroid and myeloid progenitor colonies. Two distinct *Dis3* shRNAs decreased Burst-Forming Unit-Erythroid (BFU-E) 87% and 76% (*P* < 0.0001), Colony Forming Unit-Erythroid (CFU-E) 90% and 65%, (*P* < 0.0001) and Colony Forming Unit-Granulocyte Macrophage (CFU-GM) 89% and 79% (*P* < 0.0001) compared to an shRNA targeting firefly luciferase (Luc). Bora depletion did not alter BFU-E, CFU-E or CFU-GM (Figure 2B). Flow cytometric analysis revealed that Dis3 depletion reduced the percentage of erythroid precursors (R1 population) 61% and 45% (*P* = 0.0032 and *P* = 0.0162). Bora loss did not alter erythroid maturation (Figure 2C). Although GATA1 repressed both *Dis3* and *Bora*, only Dis3 depletion, prior to GATA1-mediated repression, impaired hematopoietic progenitors.

Essential EC catalytic subunit functions in hematopoietic progenitor cells

Since Dis3 depletion compromised hematopoietic progenitors, we used a similar approach to compare Dis3 and Exosc10 functions in Lin− progenitors (Figure 3A). Under culture conditions that support erythroid precursor expansion, two Dis3 shRNAs reduced *Dis3* mRNA 82% and 73%
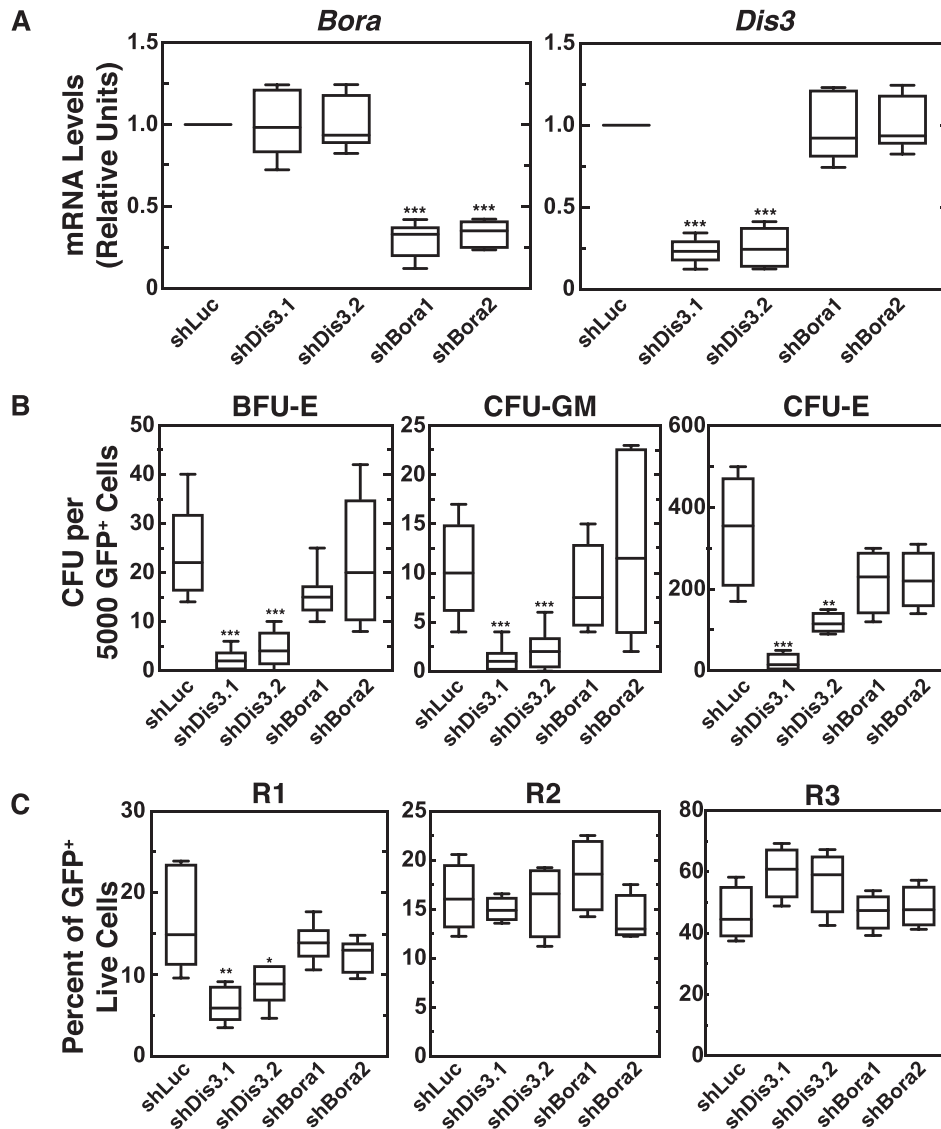
Figure 2. EC catalytic subunit Dis3, but not Bora, encoded by the neighboring gene, confers myeloid and erythroid progenitor activity. (**A**) Real-time RT-PCR analysis of mRNA levels in control versus *Dis3* or *Bora* knockdown in primary murine fetal liver. Values were normalized to 18S rRNA expression (n = 6). (**B**) CFU activity of FACS-purified GFP$^+$ fetal liver hematopoietic progenitors (n = 6). (**C**) Quantitation of flow cytometric analyses of cells cultured for 3 days in Epo, SCF-containing erythroid expansion media (n = 6). Statistically significant differences related to shLuc control are indicated *P < 0.05, **P < 0.01, ***P < 0.001 using Student's t-test.

(P < 0.0001) without affecting *Exosc10* mRNA levels. Two *Exosc10* shRNAs reduced *Exosc10* mRNA 64% and 68% (P < 0.0001) without impacting *Dis3* mRNA levels (Figure 3B). The *Dis3* and *Exosc10* mRNA decreases caused proportional declines of their proteins (Figure 3C). Thus, loss of one catalytic subunit did not alter expression of the other. GFP$^+$ erythroid progenitors (2000 CD71^{int}Ter119$^-$ cells) were purified and analyzed in a CFU assay to quantify the impact of Dis3 or Exosc10 loss. Dis3 depletion reduced CFU-E, BFU-E and CFU-GM by >80% (P < 0.0001) (Figure 3D). As the erythroid progenitors analyzed in this CFU assay were isolated from heterogenous Lin$^-$ progenitors, low numbers of CFU-GM were generated. Exosc10 depletion decreased BFU-E by 65% without altering CFU-E and CFU-GM. Thus, both EC catalytic subunits were required

for BFU-E, with the Dis3 loss-of-function phenotype being more severe.

As EC is expressed ubiquitously and a common progenitor generates erythroid and myeloid progeny, we considered whether EC activity to control erythroid differentiation is erythroid-specific or also relevant to myeloid differentiation. We tested the following models: (i) Altered Dis3/Exosc10 levels impact erythroid cells more severely than myeloid cells; (ii) Altered Dis3/Exosc10 levels impact myeloid differentiation more severely than erythroid cells, (iii) Dis3/Exosc10 are similarly important for myeloid and erythroid differentiation. Hematopoietic progenitors (4000 GFP$^+$) were analyzed in a CFU assay. Heterogeneous fetal liver Lin$^-$ progenitors generate CFU-E, BFU-E and CFU-GM. Dis3 depletion decreased BFU-E, CFU-E
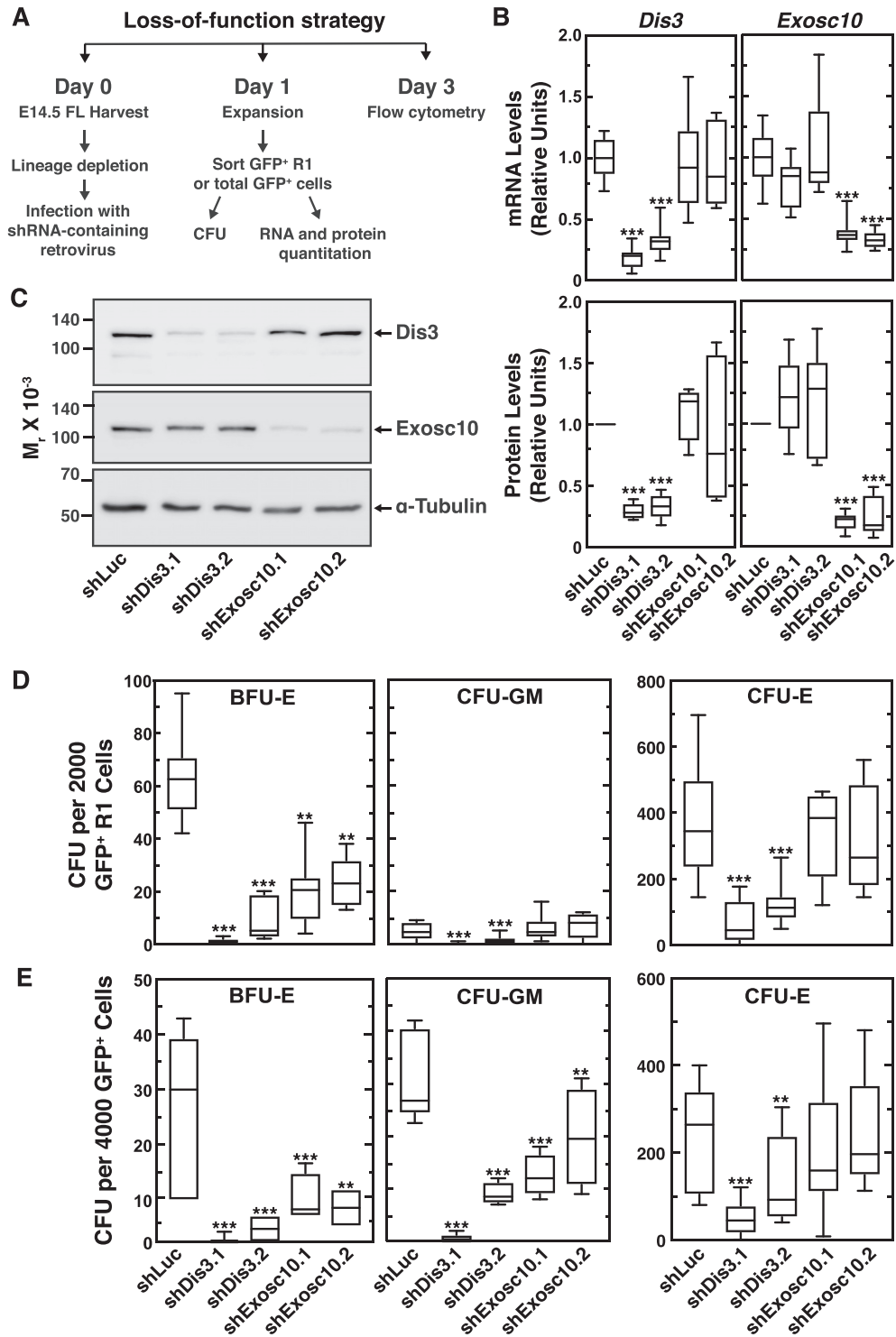
Figure 3. EC catalytic subunit requirement for BFU-E. (**A**) Experimental strategy for analyzing Dis3 and Exosc10 loss-of-function. (**B**) Real-time RT-PCR analysis of mRNAs in control, Dis3 or Exosc10 knockdown cells from murine fetal liver. Values were normalized to 18S rRNA expression ($n = 18$). (**C**) Dis3 and Exosc10 protein levels in fetal liver-derived GFP$^+$ R1 + R2 cells. Left, representative western blots; right, quantitation of Dis3 and Exosc10 protein levels in fetal liver-derived GFP$^+$ R1 + R2 cells. Values were normalized to α-tubulin ($n = 4$). (**D**) CFU activity of FACS-purified GFP$^+$ fetal liver erythroid precursors (CD71^{int}Ter119$^-$) ($n = 10$). (**E**) CFU activity of FACS-purified GFP$^+$ fetal liver hematopoietic progenitors ($n = 6$). For the box-and-whisker plots, the box depicts the 25 to 75th percentiles of data, the line represents median, and whiskers ranging from minimum to maximum values. Statistically significant differences relative to shLuc control are indicated *$P < 0.05$, **$P < 0.01$, ***$P < 0.001$ using two-tailed unpaired Student's *t*-test.

and CFU-GM. By contrast, Exosc10 depletion decreased BFU-E and CFU-GM without altering CFU-E (Figure 3E). As it is challenging to dissect mechanisms in an 8-day CFU assay, we utilized a short-term liquid culture differentiation system to further analyze EC catalytic subunit function. Lin$^-$ cells were cultured in IL-3 and SCF-containing media that supports myelo-erythroid differentiation. After infection with shRNA-expressing retroviruses (48 hours), myeloid and erythroid cell populations were quantified by flow cytometry. Dis3 depletion using two distinct shRNAs increased Mac1$^+$Gr1$^+$ double-positive cells 2-fold, without altering frequencies of single-positive cells (Figure 4A). By contrast, Dis3 depletion decreased erythroid precursors/proerythroblasts (R1 + R2) by 32% and 30%, and late basophilic/orthochromatic erythroblasts (R3) by 65% and 65% (Figure 4B). In this system, Exosc10 depletion did not impact the cell frequencies.

As Dis3 depletion compromised erythroid cells in CFU and liquid culture assays, and GATA1 represses EC subunit genes upon erythroid differentiation, we asked if EC catalytic subunit loss alters erythroid precursor differentiation capacity in a system that supports predominantly erythropoiesis. Flow cytometric analysis of cells from an erythroid culture system revealed that Dis3 depletion decreased the erythroid precursor-containing R1 population by 56% ($P = 0.0003$) and 52% ($P = 0.001$). Exosc10 depletion reduced the R1 population by 43% ($P = 0.0065$) and 34% ($P = 0.0363$) (Figure 4C). Thus, loss-of-function phenotypes from multiple systems demonstrate that EC catalytic subunits are important determinants of erythroid precursor cell levels/activities.

EC-dependent cellular survival mechanism

Given the EC functions to degrade and process RNAs, and the role of EC catalytic subunits as determinants of erythroid precursors, we tested whether Dis3 and Exosc10 depletion interferes with RNA processing and generates an aberrant transcriptome. rRNA processing intermediates accumulated with loss of either catalytic subunit (Supplementary Figure S2). For genome-wide transcriptomic analysis, GFP$^+$ erythroid precursors (CD71^{int}Ter119$^-$) and proerythroblasts (CD71$^{int/+}$Ter119$^-$) were purified from firefly luciferase, Dis3 or Exosc10 shRNA-expressing fetal liver cells. RNA-seq was conducted in quadruplicate with RNA isolated from cells sorted 2 days after erythroid expansion culture. Of the 49,081 annotated RNAs quantified from a library of rRNA-depleted total RNA, Dis3 depletion dysregulated RNAs corresponding to 57 genes, including *Dis3* (Figure 5A, B). Exosc10 depletion dysregulated *Exosc10* and six additional RNAs. Prior RNA-seq analysis of the consequences of Exosc3 or Dis3 depletion in mouse B cells and Dis3 depletion in HCT116 cells also did not describe vast mRNA changes (4,6,45).

Comparison of the Dis3-regulated coding transcripts with the GATA1-regulated transcriptome in G1E-ER-GATA1 and GATA2-regulated transcriptomes in erythroid precursor cells revealed GATA1-regulated (63%) (34), GATA2-regulated (60%) (46) or GATA1/GATA2-co-regulated (40%) Dis3-regulated transcripts (Figure 5C). Gene ontology analysis of Dis3-regulated transcripts re-

vealed regulation of cell proliferation ($P = 0.0024$) and apoptosis ($P = 0.0027$) as the top categories (Figure 5D).

EC subunit depletions differentially affect non-coding RNAs in different systems, suggesting considerable mechanistic diversity. HEK293 cells expressing a Dis3 catalytic domain mutant exhibited a 50-fold increase in PROMPTs, with little to no change in eRNAs or lncRNAs. The rapid depletion of Dis3, but not Exosc10, increased eRNAs, PROMPTs, and premature cleavage and poly-adenylation products in HCT116 colon cancer cells (6,47). *Exosc3*$^{-/-}$ B cells exhibited a greater increase in eRNAs and lncRNAs relative to antisense transcripts (4).

Given the EC function to degrade antisense transcripts, and the regulation of chromatin structure and transcription by antisense RNAs (48), we tested if Dis3 or Exosc10 depletion dysregulates antisense transcription at the transcription start sites of genes proceeding away from the coding sequence. Based on their unique, non-overlapping and most abundant transcript-producing transcription start sites, we analyzed 10,423 genes. Dis3 or Exosc10 depletion did not alter global antisense transcription relative to shLuc (Figure 5E). In pair-wise comparisons between shLuc, shDis3 and shExosc10, the most significant differences were detected in the shDis3 vs. shLuc comparison (Figure 5F). With an FDR cutoff of 0.05, Dis3 depletion significantly altered antisense RNA (asRNA) at 27 loci. 23 of the 27 (85%) asRNAs were upregulated, whereas the reads quantified from the initial exons corresponding to the differentially-expressed asRNAs did not change. shDis3 versus shLuc asRNA changes were disproportionately shifted to the right side of the volcano plot indicating positive log$_2$ fold changes for a majority of the comparisons with small, but insignificant, p-values (Figure 5F). To analyze this trend further, we plotted the distribution of the log$_2$ fold changes of loci meeting a more lenient FDR cutoff of 0.2 (Figure 5G). Increasing the FDR cutoff from 0.05 to 0.2 increased the Dis3-regulated asRNAs to 95; 82 (86%) and 13 (14%) were upregulated and downregulated, respectively. For all FDR cutoffs up to 0.5, the number of upregulated asRNAs were greater than downregulated asRNAs. By contrast, the upregulated vs. downregulated initial exons exhibited a comparable trend with an increasing FDR (Figure 5G). Figure 6A–C illustrates the significantly altered antisense RNAs (FDR < 0.05) up to 2 kb upstream of TSS. These results indicate that Dis3 depletion elevates a restricted cohort of asRNAs, and asRNAs were more sensitive to Dis3 depletion versus Exosc10 depletion.

Considering the proliferation- and apoptosis-associated genes revealed by GO analysis (Figure 5D), we analyzed mechanisms underlying the erythroid progenitor defect by quantifying erythroid progenitor and immature erythroblast proliferation and survival. Proliferation was indistinguishable between control cells and Dis3- or Exosc10-depleted cells during 48 h of expansion culture (Supplementary Figure S3). Apoptosis was quantified using Annexin V and DRAQ7-based flow cytometric analysis 72 hours post-infection. With two distinct *Dis3* shRNAs, early (3.4% to 13% and 14%) and late apoptosis (6.4% to 29% and 25%) increased in erythroid precursors (R1) (Figure 7A). In immature erythroblasts (R2), early apoptosis increased from 3.3% to 10% and 11%, and late apoptosis from 2.4% to 25%
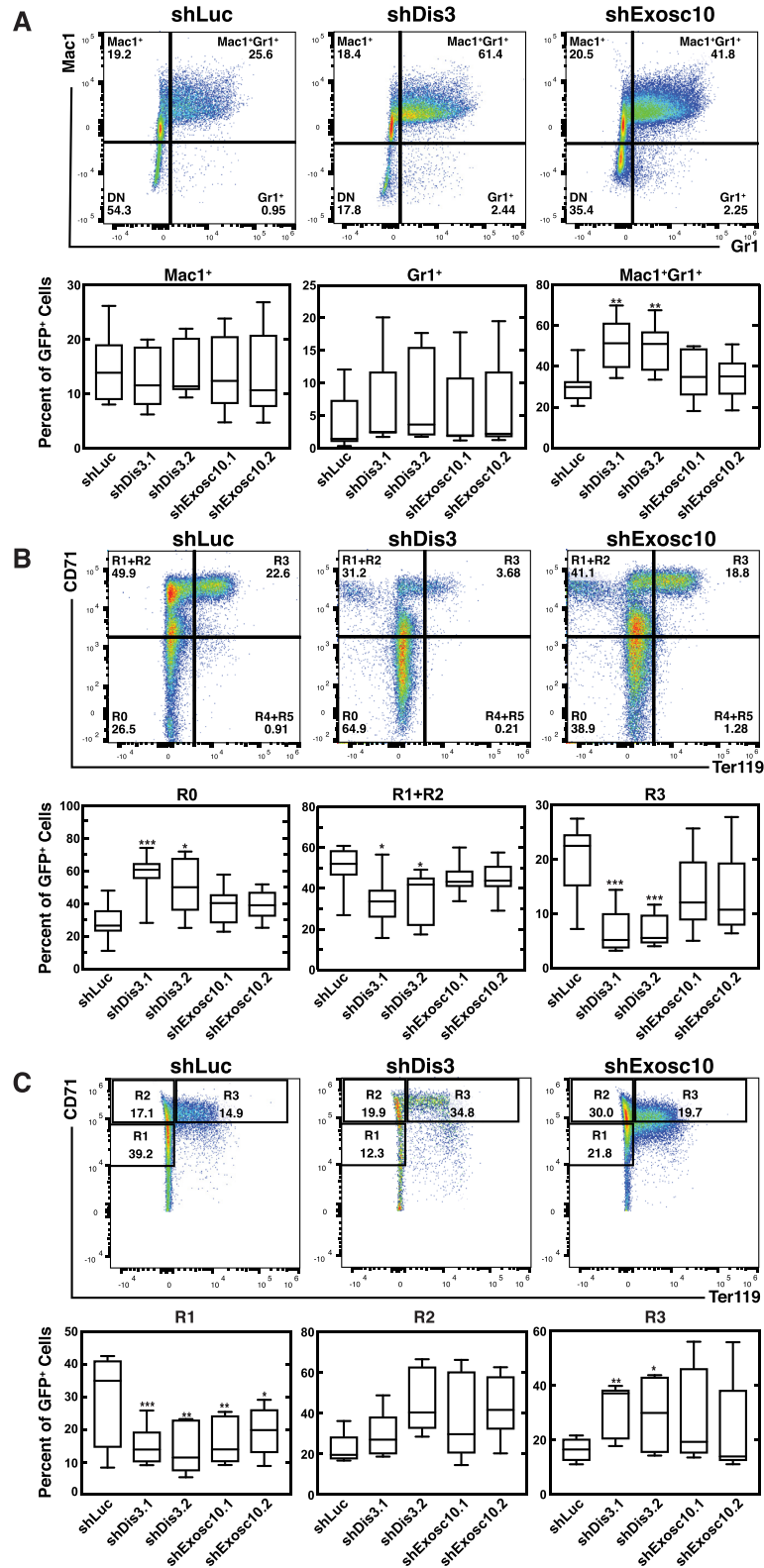
Figure 4. EC catalytic subunit Dis3 promotes erythroid differentiation. (**A**) Representative Mac1-Gr1 flow plots and quantitation of cells cultured for 3 days in IL3, SCF-containing myelo-erythroid media (n = 8). (**B**) Representative CD71-Ter119 flow plots and quantitation of cells cultured for 3 days in IL3, SCF-containing myelo-erythroid media (*n* = 8). (**C**) Representative CD71-Ter119 flow plots and quantitation of cells cultured for 3 days in Epo and SCF-containing erythroid expansion media (n = 7). For the box-and-whisker plots, the box depicts the 25–75th percentiles of data, the line represents median, and whiskers ranging from minimum to maximum values. Statistically significant differences relative to shLuc control are indicated *$P < 0.05$, **$P < 0.01$, ***$P < 0.001$ using two-tailed unpaired student's t-test.
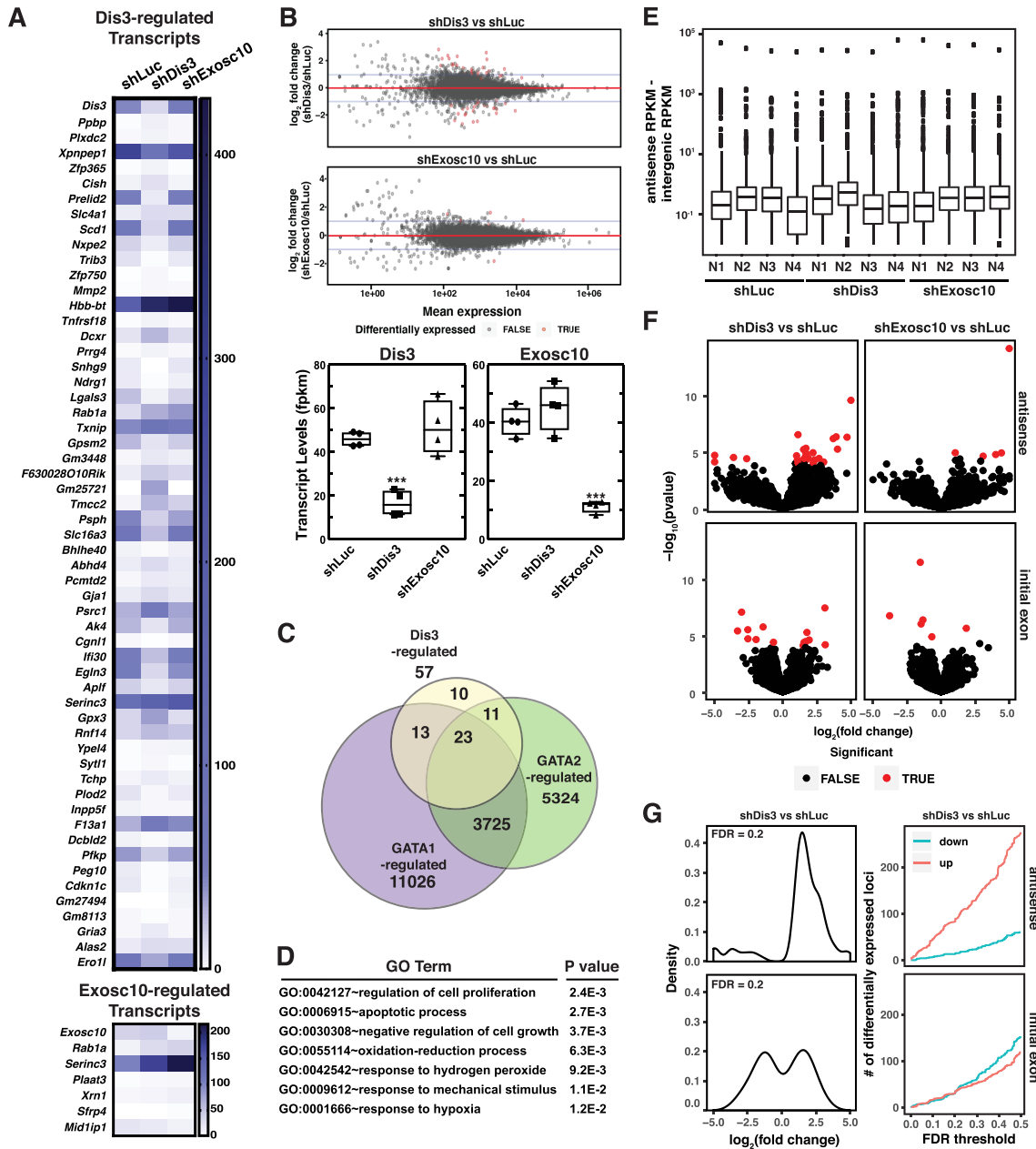
Figure 5. Restricted EC remodeling of the erythroblast transcriptome. (**A**) Heat map displaying all differentially expressed (DE) Dis3-regulated transcripts (top), and Exosc10-regulated transcripts (bottom) ($P_{adj} < 0.05$). (**B**) Top, MA-plots representing the statistical analyses between shLuc and shDis3, and shLuc and shExosc10. The red circles depict significant DE transcripts. Bottom, estimated abundances (FPKM reads) for *Dis3* and *Exosc10* mRNAs. (**C**) The Venn diagram depicts shared DE genes between Dis3, GATA2, and GATA1. (**D**) Gene ontology analysis conducted using DAVID Bioinformatics Database illustrating biological processes regulated by genes that are dysregulated by Dis3 depletion. (**E**) Distributions of antisense transcription at 10,423 unique, non-overlapping loci after subtracting intergenic read signal (background) for each replicate. (**F**) Top, volcano plots depicting Dis3-regulated (left) and Exosc10-regulated (right) asRNAs; Bottom, volcano plots depicting Dis3-regulated (left) and Exosc10-regulated (right) initial exons. (**G**) Left, distributions of fold change (shDis3 versus shLuc) for antisense and initial exon loci meeting a more lenient FDR threshold of 0.2. Right, the number of significant antisense and initial exon loci as a function of the FDR threshold for the shDis3 versus shLuc comparison.

and 21% (Figure 7B). The survival of late basophilic and orthochromatic erythroblasts was unaltered (Figure 7C), consistent with GATA1 repression of EC subunit expression upon differentiation, with little to no EC remaining in late-stage erythroblasts. Analysis with two *Exosc10* shRNAs revealed increased early apoptosis in erythroid precursors (3.4% to16% and 16%) and immature erythroblasts (3.3%

to 11% and 11%). Late apoptosis increase was also significantly greater with Dis3 loss, but not Exosc10 loss.

EC structural subunit depletion decreases cell surface c-Kit levels and *Kit* transcription (26). SCF-regulated c-Kit signaling promotes erythroblast proliferation and survival (49). We asked if EC catalytic subunits regulate surface c-Kit and if the c-Kit level correlates with apoptosis. Dis3,
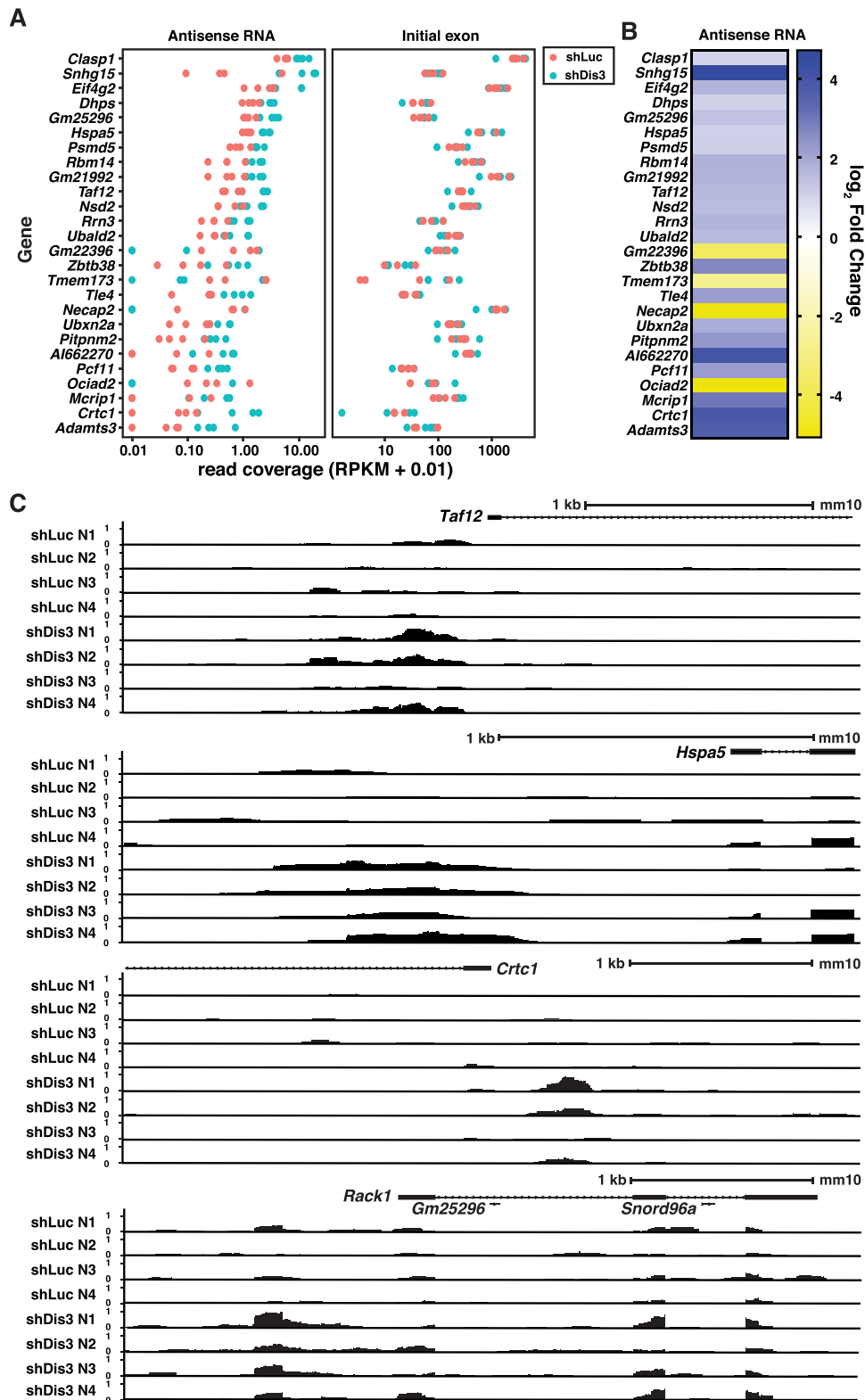
Figure 6. Dis3 regulation of antisense RNAs in erythroblasts. (**A**) Left, scatter plot illustrating RPKM values for all differentially expressed asRNA; right, corresponding initial exon RPKM values for all replicates of cells expressing shLuc and shDis3, (**B**) Heatmap illustrating log2fold changes for all differentially expressed (DE) Dis3-regulated antisense transcripts. (**C**) Antisense RNA expression profiles at select loci identified from shDis3-upregulated asRNA cohort.
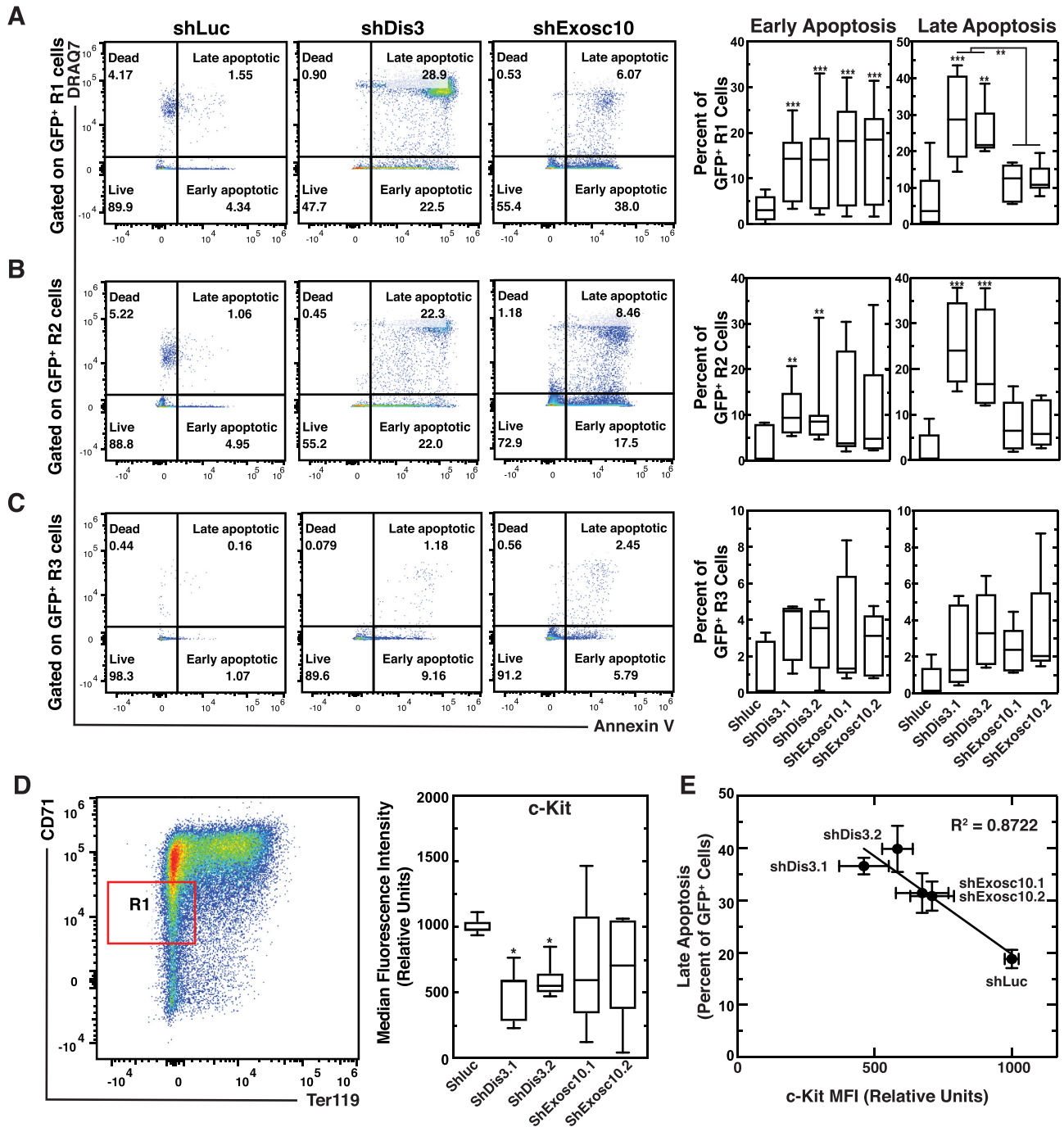
Figure 7. EC confers erythroblast survival. (**A**) Representative flow plots (left) and quantitation (right) of AnnexinV-DRAQ7-based flow cytometric apoptosis analysis in CD71^{int}Ter119^{-} erythroid precursor R1 cells (n = 7). (**B**) Representative flow plots (left) and quantitation of AnnexinV-DRAQ7-based flow cytometric apoptosis analysis in CD71^{+}Ter119^{-} proerythroblast R2 cells (*n* = 7). (**C**) Representative flow plots (left) and quantitation of AnnexinV-DRAQ7-based flow cytometric apoptosis analysis with CD71^{+}Ter119^{+} late basophilic and orthochromatic R3 erythroblasts (*n* = 7). (**D**) Cell surface c-Kit levels were quantitated in erythroid precursors using flow cytometry (*n* = 6). (**E**) Correlation plot between percent of GFP^{+} cells in late apoptosis vs. surface c-Kit levels created using linear regression (Graphpad Prism software). For the box-and-whisker plots, the box depicts the 25–75th percentiles of data, the line represents median, and whiskers ranging from minimum to maximum values. Statistically significant differences are indicated *$P < 0.05$, **$P < 0.01$, ***$P < 0.001$ using two-tailed unpaired Student's *t*-test. Values were compared to shLuc unless indicated.

but not Exosc10, depletion decreased surface c-Kit levels (Figure 7D), which negatively correlated ($R^2 = 0.8722$) with the percentage of late-apoptotic GFP$^+$ erythroid precursor cells (Figure 7E). The regulatory link between expression of Dis3, the pro-survival receptor c-Kit and erythroid precursor cell survival suggests an important EC catalytic subunit mechanism in erythroid biology.

EC protects erythroblasts against apoptosis and DNA damage

We hypothesized that precocious EC catalytic subunit loss in erythroid precursor cells, prior to GATA1-mediated repression of EC subunit genes, initiates apoptosis and renders cells hypersensitive to apoptosis-inducing stimuli. Dis3 or Exosc10 depletion induced erythroid precursor cell apoptosis (Figure 7A, B). Using staurosporine, a protein kinase inhibitor and activator of intrinsic and extrinsic apoptosis pathways, we asked if catalytic subunit loss impacts the efficacy and/or potency of staurosporine to induce apoptosis (Figure 8A). After 24 h of treatment with 1 μM staurosporine, >90% of the cells were apoptotic in control and Dis3-depleted cells. For vehicle (DMSO)-treated cells, a greater percentage of Dis3-depleted cells were apoptotic vs. control cells (Figure 8B). Staurosporine was more potent in inducing apoptosis in Dis3-depleted vs. control cells (Figure 8C). Staurosporine induced 50% of maximal apoptosis in the erythroid progenitor-enriched R1 subpopulation infected with shDis3.1 and shDis3.2 at 0.103 μM and 0.147 μM, respectively; shLuc cells required 0.289 μM. Staurosporine also induced 50% maximal apoptosis in proerythroblasts (R2) at a lower concentration in shDis3.1 (0.158 μM) and shDis3.2 (0.169 μM) infected cells vs. control cells (0.633 μM) (Figure 8C). As Dis3 depletion induced apoptosis and rendered cells hypersensitive to an apoptosis activator, Dis3 confers erythroid precursor survival prior to GATA1-mediated EC subunit gene repression.

Exosc3 or Exosc10 depletion in embryonic stem cells (ESCs) and Exosc3 depletion in B cells increased DNA double-stranded breaks (DSB), which was attributed to R-loop accumulation at loci in which transcription occurs in sense and antisense directions, relative to promoters (4,50). R-loops form between a nascent RNA strand and its DNA template strand (51,52). As EC degrades the RNA component, EC subunit depletion may increase R-loops and DNA damage. DSB-induced genome instability can trigger cell cycle arrest, DNA repair machinery recruitment, and apoptosis. Since many questions remain regarding mechanisms conferring genomic integrity during the massive proliferation of erythroid precursors and their progressive maturation, we asked if EC catalytic subunits are determinants of genomic stability by quantifying DSB-associated γ-H2AX in control and Dis3- or Exosc10-depleted erythroblasts (Figure 8D). Dis3 depletion increased γ-H2AX 7.7- and 23-fold at 24 and 36 h, respectively, under conditions in which nuclear and cell morphology, based on DAPI and GFP staining, were unaltered. Exosc10 depletion did not alter γ-H2AX at 24 and 36 hours (Figure 8D). At 48 hours, Dis3 or Exosc10 depletion increased γ-H2AX 12- and 8.2-fold, respectively. The EC catalytic subunit activity

to suppress γ-H2AX supports a role for the catalytic subunits in promoting genomic integrity and survival of erythroid precursor cells.

Multiple myeloma-linked Dis3 disease mutations disrupt Dis3-dependent progenitor cell regulation

Human *DIS3* is mutated recurrently in multiple myeloma, and *DIS3* mutations have been detected in acute myeloid leukemia (AML) and other cancer types (12,53). These mutations are proposed to be loss-of-function based on loss of heterozygosity in tumor cells, and catalytic domain disease mutations analyzed in yeast and HEK293 cells exhibit reduced exoribonuclease activity (54). As many questions remain regarding the mechanistic consequences of *DIS3* mutations, and disease mutations can reveal unique mechanistic insights, we innovated a genetic rescue assay to compare the activities of Dis3 S447R and R750K disease mutants, which have alterations in the catalytic RNB domain (Figure 9A). shRNA-resistant wild type or mutant human Dis3 was co-expressed with mouse Dis3-targeting shRNA. To isolate cells harboring both vectors, we used GFP and mCherry as markers for shRNA-containing and cDNA-containing retroviruses, respectively (Figure 9B). GFP$^+$mCherry$^+$ cells expressing shRNA and expression vector were isolated by FACS, and proteins were analyzed by semi-quantitative Western blotting. HA-Dis3(WT), HA-Dis3(S447R) and HA-Dis3(R750K) levels resembled that of endogenous murine Dis3 (Figure 9C). shDis3 depleted endogenous Dis3 by 78% ($P < 0.00001$), and the expressed proteins exhibited a normal nuclear localization (Figure 9D).

We asked if human Dis3 disease mutants rescue the erythroid CFU defect caused by Dis3 depletion. While Dis3(WT) expression rescued BFU-E and CFU-E up to 60% of the control, Dis3(S447R) and Dis3(R750K) mutants lacked activity (Figure 9E). Thus, human *DIS3* disease mutants with catalytic domain alterations are unable to support the generation/activity of erythroid progenitor cells. In aggregate, these results revealed a mechanism in which EC catalytic subunits confer erythroid precursor cell survival. The erythroid precursor cells are more sensitive to Dis3 versus Exosc10 depletion, and *DIS3* human disease mutations abrogate the regulatory activity of Dis3 (Figure 10).

DISCUSSION

Central to the intricate mechanism by which the EC degrades and processes RNAs is the selective recognition of specific RNAs. Based on ubiquitous EC expression in diverse cell types, one would assume that EC activities are vitally integrated into a plethora of biological processes. However, the cell type-specific cofactors mediating RNA recognition (55,56) portend EC functions unique to distinct biological systems and/or processes within a system. Previously, we described an EC mechanism to balance erythroblast proliferation vs. differentiation (26). EC structural subunit loss compromised the maintenance of BFU-E and increased mature progeny. This primary cell differentiation system, in which progenitors with multi-lineage potential undergo myeloid or erythroid differentiation *ex vivo* (27),
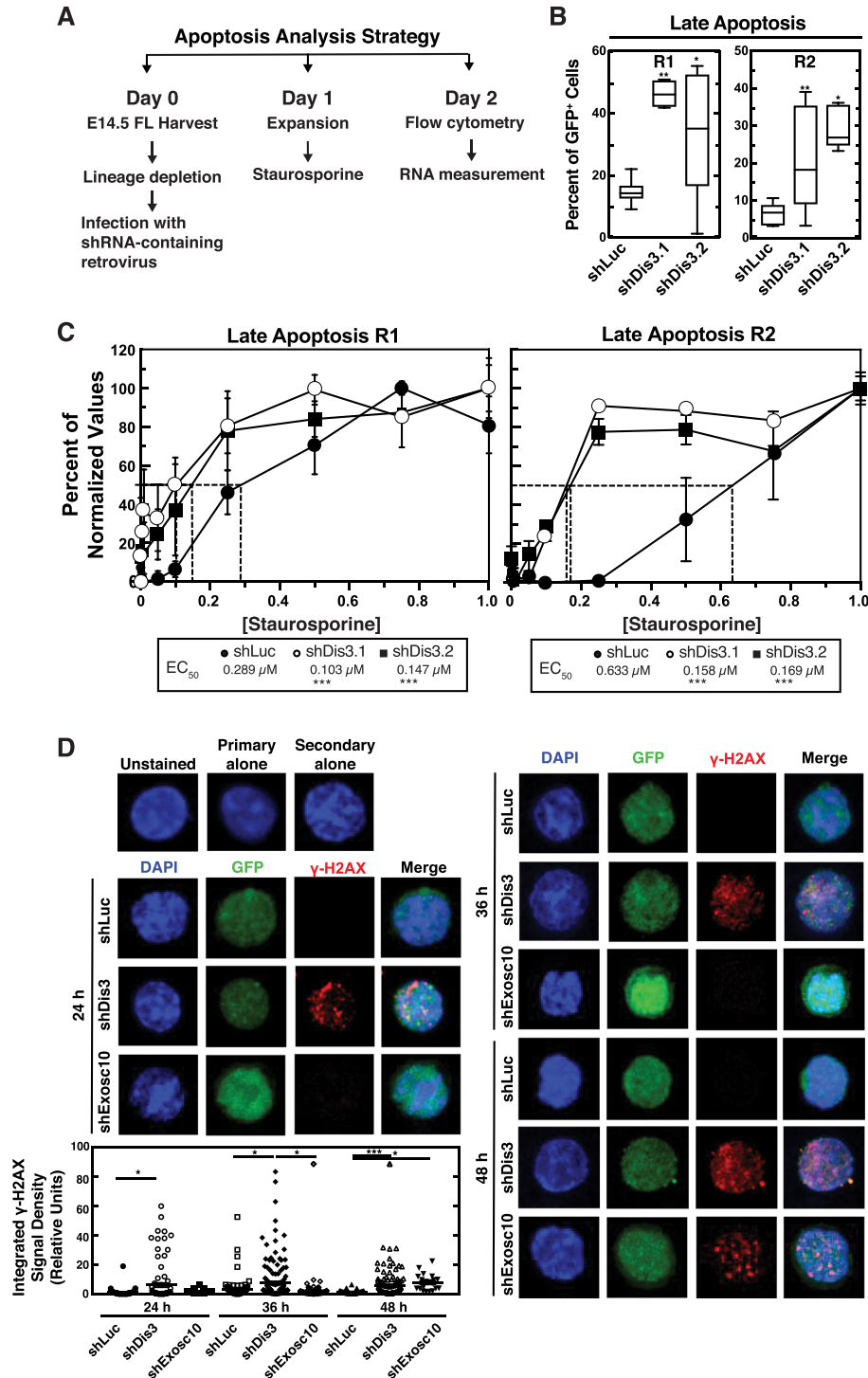
Figure 8. EC suppresses erythroblast apoptosis and DNA damage. (**A**) Staurosporine treatment and apoptosis analysis strategy. (**B**) Quantitation of AnnexinV⁺DRAQ7⁺ late apoptotic cells in erythroid precursors (R1) and proerythroblasts (R2) with DMSO treatment ($n = 6$). (**C**) Normalized quantitation of AnnexinV-DRAQ7-based flow cytometric apoptosis analysis in erythroid precursors (R1) and proerythroblasts (R2) with increasing concentrations of staurosporine. The data represent mean ± SEM ($n = 6$). (**D**) Cells were harvested 24, 36, and 48 h post-infection, plated on poly-lysine coated slides and stained with anti-γ-H2AX and DAPI. γ-H2AX (Ser139) was visualized by confocal microscope (Nikon A1RS Confocal Imaging System). Magnification (100X). Integrated γ-H2AX signal density in GFP⁺ cells was quantified using FIJI (28) ($n = 100$ cells per condition. For (**B**) and (**C**), statistically significant differences are indicated *$P < 0.05$, **$P < 0.01$, ***$P < 0.001$ using two-tailed unpaired Student's t-test. For (**D**), statistically significant differences are indicated *$P < 0.05$, **$P < 0.01$, ***$P < 0.001$ using Kruskal–Wallis test using Prism by Graphpad software.
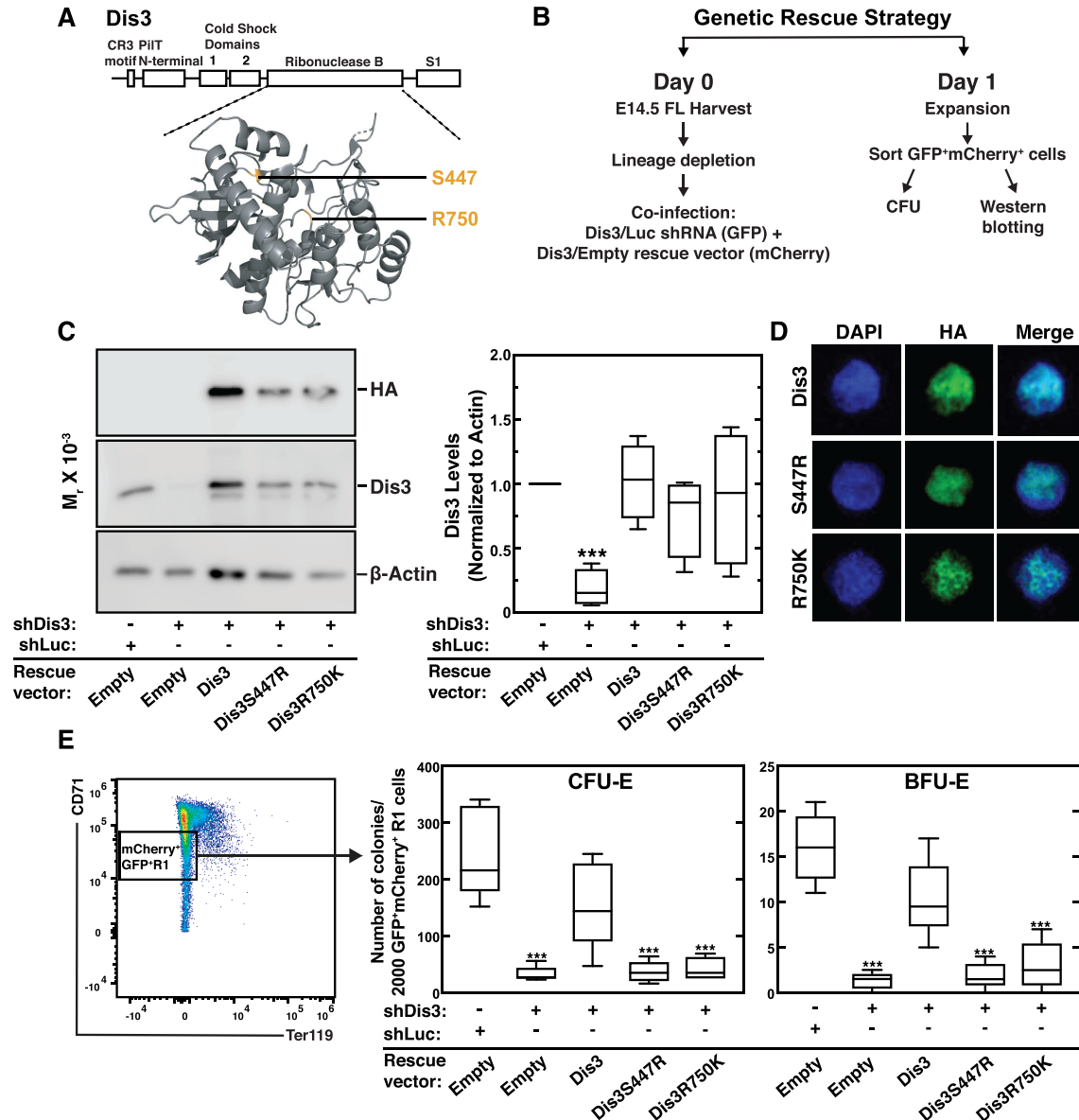
Figure 9. Rescue of erythroid progenitors by Dis3, but not multiple myeloma-associated Dis3 mutants. (**A**) Dis3 RNB domain structural model based on human Dis3 crystal structure (10). (**B**) Dis3 genetic rescue strategy. (**C**) Left, representative Western blots; right, quantitation of Dis3 protein in fetal liver-derived mCherry$^+$GFP$^+$ cells. Values were normalized to β-actin ($n = 5$). (**D**) Immunofluorescence analysis with anti-HA antibody in primary cells expressing HA-Dis3 and mutant proteins. (**E**) CFU activity of FACS-purified GFP$^+$ erythroid precursors (CD71^{int}Ter119$^-$) ($n = 5$). Statistically significant differences are indicated *$P < 0.05$, **$P < 0.01$, ***$P < 0.001$ using two-tailed unpaired Student's t-test.

allows one to analyze EC functions in a dynamic differentiation process. Herein, we demonstrated that the EC suppresses erythroblast apoptosis in the steady-state and circumscribes the response to a pro-apoptotic stimulus. The survival mechanism required EC catalytic subunits, with cells being more sensitive to Dis3 loss than Exosc10. Depleting catalytic subunits compromised erythroid, while sparing Mac1$^+$Gr1$^+$ myeloid cell progeny in an *ex vivo* culture assay. Dis3 depletion also did not compromise B-cell survival (39). These results support a paradigm in which cell-type specific EC functions suppress DNA damage and apoptosis and confer survival, explaining why EC disruption depletes BFU-E.

GATA1 is essential for erythropoiesis and confers erythroblast survival (57–59). Erythropoietin receptor (EpoR) signaling cooperates with GATA1 to upregulate the anti-apoptotic factor Bcl-XL (35). GATA1 utilizes the histone methyltransferase and corepressor SetD8 at select target genes, and SetD8 promotes erythroblast survival in CD71$^+$Ter119$^+$ murine erythroblasts (60–62). GATA1 induces expression of the equilibrative nucleoside transporter Slc29a1 that transports adenosine (63). Slc29a1 regulates adenosine-dependent processes and confers erythroblast survival (63). SCF activates c-Kit signaling, which synergizes with EpoR signaling to promote survival and proliferation of erythroblasts (64). GATA1 represses *Kit* tran-
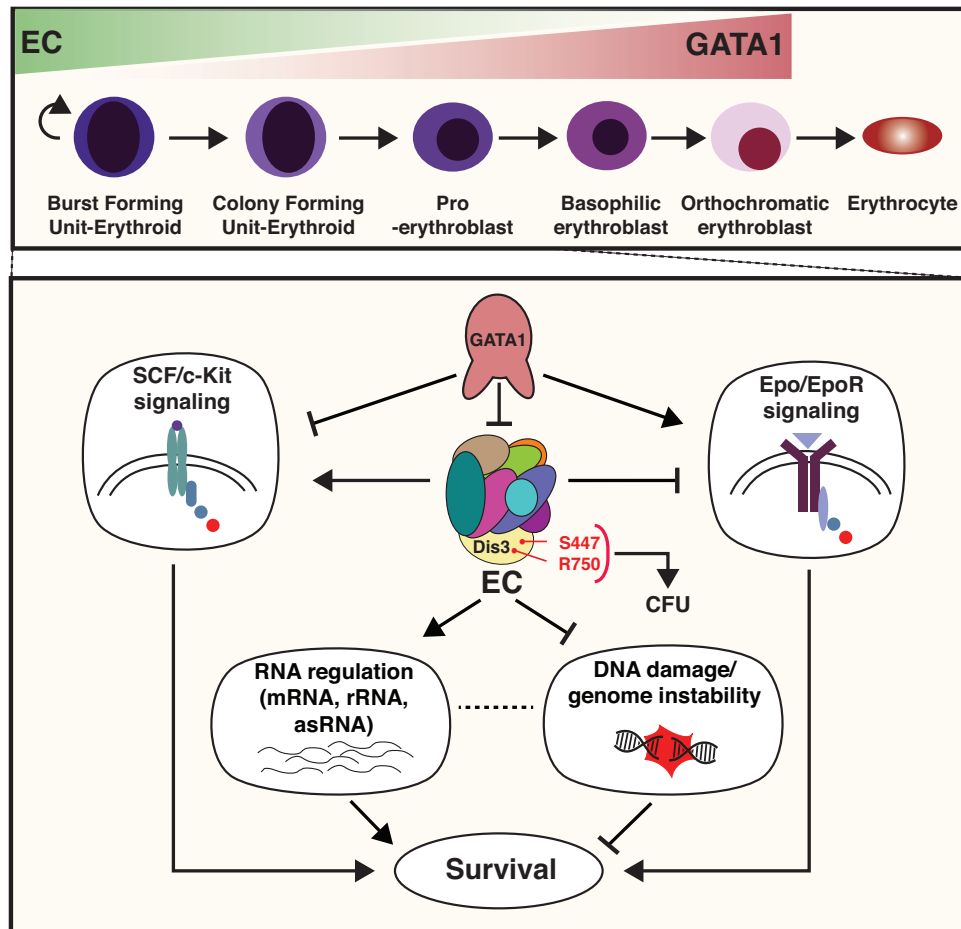
Figure 10. Model of EC-regulated erythroid precursor survival and differentiation. The EC confers survival to erythroid precursors and immature erythroblasts, prior to GATA1-mediated repression of genes encoding EC subunits. Under these conditions, EC catalytic activity suppresses DNA damage, thus promoting genome stability. Dis3 depletion dysregulates a restricted cohort of mRNAs and RNAs accumulate aberrantly, including rRNA intermediates and antisense RNAs. These data support a model in which the EC RNA-regulatory mechanism promotes erythroid precursor survival and proliferation, in part by elevating SCF/c-Kit signaling, protecting against DNA damage and maintaining genomic stability, while inhibiting differentiation driven by pro-differentiation Epo/EpoR signaling (24,26).

scription upon differentiation (65,66), which abolishes c-Kit signaling and enables pro-differentiation signaling to prevail (26). Analogous to GATA1 repressing *Kit*, GATA1 represses EC subunit genes, which also favors erythroid precursor maintenance (25,26), and Dis3 depletion induces a proportional loss of c-Kit (Figure 7E). Thus, the EC-c-Kit axis operates prior to GATA1-mediated repression of EC subunit genes and differentiation. EC catalytic subunits conferred survival in erythroid precursors, and EC catalytic subunit depletion did not impact Bcl-XL expression.

Although Dis3 and Exosc10 both have 3′-5′ exonucleolytic activity, our studies revealed differential consequences of depleting these subunits. Dis3 depletion abrogated BFU-E and CFU-E, triggered early and late apoptosis, reduced cell-surface c-Kit, rapidly increased DNA damage, and elevated rRNA processing intermediates. Dis3 expression rescued defects, while Dis3 human disease mutants were inactive, despite normal expression levels. Exosc10 depletion decreased, without ablating, BFU-E, increased early apoptosis, and elevated DNA damage with

slower kinetics and to a lesser extent than with Dis3 depletion. Transcriptomic analysis revealed restricted coding and non-coding transcript alterations upon depletion of either subunit, yet Dis3-regulated 8-fold more mRNAs than Exosc10. Genome-wide pervasive transcription yields non-coding transcripts, including enhancer RNAs, PROMPTs and other lncRNAs that can regulate chromatin, transcription, and post-transcriptional processes (67,68). The restricted cohort of coding and non-coding transcripts sensitive to Dis3 depletion may relate to the system, which allows one to strongly reduce, without eliminating, protein expression and therefore to identify the processes more sensitive to protein perturbations, rather than absolute loss. We predict that the most sensitive genes/proteins, including, but not limited to, c-Kit constitute key components of the EC-dependent mechanism to support erythroid precursor survival.

In summary, we provide evidence for a mechanism involving cell type-specific EC catalytic subunit functions to control cellular survival in the context of erythroid biology.

Dis3 human disease mutants accumulated normally in cells, but were functionally inactive in a genetic rescue system. It will therefore be instructive to build upon the foundation established herein by conducting detailed structure/function analyses, assessing whether loss-of-function phenotypes reflect impaired EC function or potential EC-independent activities, pinpointing EC-dependent network components with essential activities to control erythrocyte development and ascertaining the relationship between these components and those operating in diverse biological systems. Such studies will further inform post-transcriptional mechanisms governing cellular survival and differentiation, as well as relationships between the EC RNA-regulatory machine and diseases of the hematopoietic system.

DATA AVAILABILITY

Our RNA-seq data have been deposited with Gene Expression Omnibus (GEO), accession numbers: GSE167090. Representative flow data for each experiment has been deposited on FlowRepository Database, accession number: FR-FCM-Z3GK. All RT-PCR experiments were performed in compliance with the MIQE guidelines.

SUPPLEMENTARY DATA

Supplementary Data are available at NAR Online.

REFERENCES

1. Mitchell,P., Petfalski,E., Shevchenko,A., Mann,M. and Tollervey,D. (1997) The exosome: a conserved eukaryotic RNA processing complex containing multiple 3'→5' exoribonucleases. *Cell*, **91**, 457–466.
2. Anderson,J.S. and Parker,R.P. (1998) The 3' to 5' degradation of yeast mRNAs is a general mechanism for mRNA turnover that requires the SKI2 DEVH box protein and 3' to 5' exonucleases of the exosome complex. *EMBO J.*, **17**, 1497–1506.
3. Allmang,C., Petfalski,E., Podtelejnikov,A., Mann,M., Tollervey,D. and Mitchell,P. (1999) The yeast exosome and human PM-Scl are related complexes of 3' → 5' exonucleases. *Genes Dev.*, **13**, 2148–2158.
4. Pefanis,E., Wang,J., Rothschild,G., Lim,J., Kazadi,D., Sun,J., Federation,A., Chao,J., Elliott,O., Liu,Z.P. *et al.* (2015) RNA exosome-regulated long non-coding RNA transcription controls super-enhancer activity. *Cell*, **161**, 774–789.
5. Belair,C., Sim,S., Kim,K.Y., Tanaka,Y., Park,I.H. and Wolin,S.L. (2019) The RNA exosome nuclease complex regulates human embryonic stem cell differentiation. *J. Cell Biol.*, **218**, 2564–2582.
6. Davidson,L., Francis,L., Cordiner,R.A., Eaton,J.D., Estell,C., Macias,S., Caceres,J.F. and West,S. (2019) Rapid depletion of DIS3, EXOSC10, or XRN2 reveals the immediate impact of exoribonucleolysis on nuclear RNA metabolism and transcriptional control. *Cell Rep.*, **26**, 2779–2791.
7. Tomecki,R., Kristiansen,M.S., Lykke-Andersen,S., Chlebowski,A., Larsen,K.M., Szczesny,R.J., Drazkowska,K., Pastula,A., Andersen,J.S., Stepien,P.P. *et al.* (2010) The human core exosome interacts with differentially localized processive RNases: hDIS3 and hDIS3L. *EMBO J.*, **29**, 2342–2357.
8. Liu,Q., Greimann,J.C. and Lima,C.D. (2006) Reconstitution, activities, and structure of the eukaryotic RNA exosome. *Cell*, **127**, 1223–1237.
9. Wasmuth,E.V., Januszyk,K. and Lima,C.D. (2014) Structure of an Rrp6-RNA exosome complex bound to poly(A) RNA. *Nature*, **511**, 435–439.
10. Weick,E.M., Puno,M.R., Januszyk,K., Zinder,J.C., DiMattia,M.A. and Lima,C.D. (2018) Helicase-dependent RNA decay illuminated by a cryo-EM structure of a human nuclear RNA exosome-MTR4 complex. *Cell*, **173**, 1663–1677.
11. Kilchert,C., Wittmann,S. and Vasiljeva,L. (2016) The regulation and functions of the nuclear RNA exosome complex. *Nat. Rev. Mol. Cell Biol.*, **17**, 227–239.
12. Fraga de Andrade,I., Mehta,C. and Bresnick,E.H. (2020) Post-transcriptional control of cellular differentiation by the RNA exosome complex. *Nucleic. Acids. Res.*, **48**, 11913–11928.
13. Mitchell,P., Petfalski,E., Houalla,R., Podtelejnikov,A., Mann,M. and Tollervey,D. (2003) Rrp47p is an exosome-associated protein required for the 3' processing of stable RNAs. *Mol. Cell. Biol.*, **23**, 6982–6992.
14. Briggs,M.W., Burkard,K.T. and Butler,J.S. (1998) Rrp6p, the yeast homologue of the human PM-Scl 100-kDa autoantigen, is essential for efficient 5.8 S rRNA 3' end formation. *J. Biol. Chem.*, **273**, 13255–13263.
15. Schneider,C., Leung,E., Brown,J. and Tollervey,D. (2009) The N-terminal PIN domain of the exosome subunit Rrp44 harbors endonuclease activity and tethers Rrp44 to the yeast core exosome. *Nucleic. Acids. Res.*, **37**, 1127–1140.
16. Stead,J.A., Costello,J.L., Livingstone,M.J. and Mitchell,P. (2007) The PMC2NT domain of the catalytic exosome subunit Rrp6p provides the interface for binding with its cofactor Rrp47p, a nucleic acid-binding protein. *Nucleic Acids Res.*, **35**, 5556–5567.
17. Phillips,S. and Butler,J.S. (2003) Contribution of domain structure to the RNA 3' end processing and degradation functions of the nuclear exosome subunit Rrp6p. *RNA*, **9**, 1098–1107.
18. Januszyk,K. and Lima,C.D. (2014) The eukaryotic RNA exosome. *Curr. Opin. Struct. Biol.*, **24**, 132–140.
19. van Hoof,A., Lennertz,P. and Parker,R. (2000) Yeast exosome mutants accumulate 3'-extended polyadenylated forms of U4 small nuclear RNA and small nucleolar RNAs. *Mol. Cell. Biol.*, **20**, 441–452.
20. Staals,R.H., Bronkhorst,A.W., Schilders,G., Slomovic,S., Schuster,G., Heck,A.J., Raijmakers,R. and Pruijn,G.J. (2010) Dis3-like 1: a novel exoribonuclease associated with the human exosome. *EMBO J.*, **29**, 2358–2367.
21. Mistry,D.S., Chen,Y. and Sen,G.L. (2012) Progenitor function in self-renewing human epidermis is maintained by the exosome. *Cell Stem Cell*, **11**, 127–135.
22. Tsai,S.F., Martin,D.I., Zon,L.I., D'Andrea,A.D., Wong,G.G. and Orkin,S.H. (1989) Cloning of cDNA for the major DNA-binding protein of the erythroid lineage through expression in mammalian cells. *Nature*, **339**, 446–451.
23. Evans,T. and Felsenfeld,G. (1989) The erythroid-specific transcription factor Eryf1: a new finger protein. *Cell*, **58**, 877–885.
24. Katsumura,K.R., Bresnick,E.H. and Group,G.F.M. (2017) The GATA factor revolution in hematology. *Blood*, **129**, 2092–2102.
25. McIver,S.C., Kang,Y.A., DeVilbiss,A.W., O'Driscoll,C.A., Ouellette,J.N., Pope,N.J., Camprecios,G., Chang,C.J., Yang,D.,

Bouhassira,E.E. *et al.* (2014) The exosome complex establishes a barricade to erythroid maturation. *Blood*, **124**, 2285–2297.

26. McIver,S.C., Katsumura,K.R., Davids,E., Liu,P., Kang,Y.A., Yang,D. and Bresnick,E.H. (2016) Exosome complex orchestrates developmental signaling to balance proliferation and differentiation during erythropoiesis. *Elife*, **5**, e17877.

27. McIver,S.C., Hewitt,K.J., Gao,X., Mehta,C., Zhang,J. and Bresnick,E.H. (2018) Dissecting regulatory mechanisms using mouse fetal liver-derived erythroid cells. *Methods Mol. Biol.*, **1698**, 67–89.

28. Schindelin,J., Arganda-Carreras,I., Frise,E., Kaynig,V., Longair,M., Pietzsch,T., Preibisch,S., Rueden,C., Saalfeld,S., Schmid,B. *et al.* (2012) Fiji: an open-source platform for biological-image analysis. *Nat. Methods*, **9**, 676–682.

29. Li,B. and Dewey,C.N. (2011) RSEM: accurate transcript quantification from RNA-Seq data with or without a reference genome. *BMC Bioinformatics*, **12**, 323.

30. Dobin,A., Davis,C.A., Schlesinger,F., Drenkow,J., Zaleski,C., Jha,S., Batut,P., Chaisson,M. and Gingeras,T.R. (2013) STAR: ultrafast universal RNA-seq aligner. *Bioinformatics*, **29**, 15–21.

31. Love,M.I., Huber,W. and Anders,S. (2014) Moderated estimation of fold change and dispersion for RNA-seq data with DESeq2. *Genome Biol.*, **15**, 550.

32. Lawrence,M., Gentleman,R. and Carey,V. (2009) rtracklayer: an R package for interfacing with genome browsers. *Bioinformatics*, **25**, 1841–1842.

33. Tanimura,N., Liao,R., Wilson,G.M., Dent,M.R., Cao,M., Burstyn,J.N., Hematti,P., Liu,X., Zhang,Y., Zheng,Y. *et al.* (2018) GATA/heme multi-omics reveals a trace metal-dependent cellular differentiation mechanism. *Dev. Cell*, **46**, 581–594.

34. Tanimura,N., Miller,E., Igarashi,K., Yang,D., Burstyn,J.N., Dewey,C.N. and Bresnick,E.H. (2016) Mechanism governing heme synthesis reveals a GATA factor/heme circuit that controls differentiation. *EMBO Rep.*, **17**, 249–265.

35. Gregory,T., Yu,C., Ma,A., Orkin,S.H., Blobel,G.A. and Weiss,M.J. (1999) GATA-1 and erythropoietin cooperate to promoter erythroid cell survival by regulating bcl-xl expression. *Blood*, **94**, 87–96.

36. Welch,J.J., Watts,J.A., Vakoc,C.R., Yao,Y., Wang,H., Hardison,R.C., Blobel,G.A., Chodosh,L.A. and Weiss,M.J. (2004) Global regulation of erythroid gene expression by transcription factor GATA-1. *Blood*, **104**, 3136–3147.

37. Hutterer,A., Berdnik,D., Wirtz-Peitz,F., Zigman,M., Schleiffer,A. and Knoblich,J.A. (2006) Mitotic activation of the kinase Aurora-A requires its binding partner Bora. *Dev. Cell*, **11**, 147–157.

38. Liao,R., Zheng,Y., Liu,X., Zhang,Y., Seim,G., Tanimura,N., Wilson,G.M., Hematti,P., Coon,J.J., Fan,J. *et al.* (2020) Discovering how heme controls genome function through heme-omics. *Cell Rep.*, **31**, 107832.

39. Wu,W., Cheng,Y., Keller,C.A., Ernst,J., Kumar,S.A., Mishra,T., Morrissey,C., Dorman,C.M., Chen,K.B., Drautz,D. *et al.* (2011) Dynamics of the epigenetic landscape during erythroid differentiation after GATA1 restoration. *Genome Res.*, **21**, 1659–1671.

40. Kang,Y.A., Sanalkumar,R., O'Geen,H., Linnemann,A.K., Chang,C.J., Bouhassira,E.E., Farnham,P.J., Keles,S. and Bresnick,E.H. (2012) Autophagy driven by a master regulator of hematopoiesis. *Mol. Cell. Biol.*, **32**, 226–239.

41. Beck,D., Thoms,J.A., Perera,D., Schutte,J., Unnikrishnan,A., Knezevic,K., Kinston,S.J., Wilson,N.K., O'Brien,T.A., Gottgens,B. *et al.* (2013) Genome-wide analysis of transcriptional regulators in human HSPCs reveals a densely interconnected network of coding and noncoding genes. *Blood*, **122**, e12–e22.

42. Wozniak,R.J., Keles,S., Lugus,J.J., Young,K., Boyer,M.E., Tran,T.T., Choi,K. and Bresnick,E.H. (2008) Molecular hallmarks of endogenous chromatin complexes containing master regulators of hematopoiesis. *Mol. Cell. Biol.*, **28**, 6681–6694.

43. Fujiwara,T., O'Geen,H., Keles,S., Blahnik,K., Linnemann,A.K., Kang,Y.A., Choi,K., Farnham,P.J. and Bresnick,E.H. (2009) Discovering hematopoietic mechanisms through genome-wide analysis of GATA factor chromatin occupancy. *Mol. Cell*, **36**, 667–681.

44. Goldenson,B., Kirsammer,G., Stankiewicz,M.J., Wen,Q.J. and Crispino,J.D. (2015) Aurora kinase A is required for hematopoiesis but is dispensable for murine megakaryocyte endomitosis and differentiation. *Blood*, **125**, 2141–2150.

45. Laffleur,B., Lim,J., Zhang,W., Chen,Y., Pefanis,E., Bizarro,J., Batista,C.R., Wu,L., Economides,A.N., Wang,J. *et al.* (2021) Noncoding RNA processing by DIS3 regulates chromosomal architecture and somatic hypermutation in B cells. *Nat. Genet.*, **53**, 230–242.

46. Mehta,C., Johnson,K.D., Gao,X., Ong,I.M., Katsumura,K.R., McIver,S.C., Ranheim,E.A. and Bresnick,E.H. (2017) Integrating enhancer mechanisms to establish a hierarchical blood development program. *Cell Rep.*, **20**, 2966–2979.

47. Szczepinska,T., Kalisiak,K., Tomecki,R., Labno,A., Borowski,L.S., Kulinski,T.M., Adamska,D., Kosinska,J. and Dziembowski,A. (2015) DIS3 shapes the RNA polymerase II transcriptome in humans by degrading a variety of unwanted transcripts. *Genome Res.*, **25**, 1622–1633.

48. Pelechano,V. and Steinmetz,L.M. (2013) Gene regulation by antisense transcription. *Nat. Rev. Genet.*, **14**, 880–893.

49. Munugalavadla,V. and Kapur,R. (2005) Role of c-Kit and erythropoietin receptor in erythropoiesis. *Crit. Rev. Oncol. Hematol.*, **54**, 63–75.

50. Pefanis,E., Wang,J., Rothschild,G., Lim,J., Chao,J., Rabadan,R., Economides,A.N. and Basu,U. (2014) Noncoding RNA transcription targets AID to divergently transcribed loci in B cells. *Nature*, **514**, 389–393.

51. Crossley,M.P., Bocek,M. and Cimprich,K.A. (2019) R-loops as cellular regulators and genomic threats. *Mol. Cell*, **73**, 398–411.

52. Hegazy,Y.A., Fernando,C.M. and Tran,E.J. (2020) The balancing act of R-loop biology: The good, the bad, and the ugly. *J. Biol. Chem.*, **295**, 905–913.

53. Chapman,M.A., Lawrence,M.S., Keats,J.J., Cibulskis,K., Sougnez,C., Schinzel,A.C., Harview,C.L., Brunet,J.P., Ahmann,G.J., Adli,M. *et al.* (2011) Initial genome sequencing and analysis of multiple myeloma. *Nature*, **471**, 467–472.

54. Tomecki,R., Drazkowska,K., Kucinski,I., Stodus,K., Szczesny,R.J., Gruchota,J., Owczarek,E.P., Kalisiak,K. and Dziembowski,A. (2014) Multiple myeloma-associated hDIS3 mutations cause perturbations in cellular RNA metabolism and suggest hDIS3 PIN domain as a potential drug target. *Nucleic. Acids. Res.*, **42**, 1270–1290.

55. Chen,C.Y., Gherzi,R., Ong,S.E., Chan,E.L., Raijmakers,R., Pruijn,G.J., Stoecklin,G., Moroni,C., Mann,M. and Karin,M. (2001) AU binding proteins recruit the exosome to degrade ARE-containing mRNAs. *Cell*, **107**, 451–464.

56. Meola,N., Domanski,M., Karadoulama,E., Chen,Y., Gentil,C., Pultz,D., Vitting-Seerup,K., Lykke-Andersen,S., Andersen,J.S., Sandelin,A. *et al.* (2016) Identification of a Nuclear Exosome Decay Pathway for Processed Transcripts. *Mol. Cell*, **64**, 520–533.

57. Weiss,M.J. and Orkin,S.H. (1995) Transcription factor GATA-1 permits survival and maturation of erythroid precursors by preventing apoptosis. *Proc. Natl. Acad. Sci. U.S.A.*, **92**, 9623–9627.

58. Pevny,L., Simon,M.C., Robertson,E., Klein,W.H., Tsai,S.F., D'Agati,V., Orkin,S.H. and Costantini,F. (1991) Erythroid differentiation in chimaeric mice blocked by a targeted mutation in the gene for transcription factor GATA-1. *Nature*, **349**, 257–260.

59. Simon,M.C., Pevny,L., Wiles,M.V., Keller,G., Costantini,F. and Orkin,S.H. (1992) Rescue of erythroid development in gene targeted GATA-1- mouse embryonic stem cells. *Nat. Genet.*, **1**, 92–98.

60. Malik,J., Lillis,J.A., Couch,T., Getman,M. and Steiner,L.A. (2017) The Methyltransferase Setd8 Is Essential for Erythroblast Survival and Maturation. *Cell Rep.*, **21**, 2376–2383.

61. DeVilbiss,A.W., Boyer,M.E. and Bresnick,E.H. (2013) Establishing a hematopoietic genetic network through locus-specific integration of chromatin regulators. *Proc. Natl. Acad. Sci. U.S.A.*, **110**, E3398–E3407.

62. DeVilbiss,A.W., Sanalkumar,R., Hall,B.D., Katsumura,K.R., de Andrade,I.F. and Bresnick,E.H. (2015) Epigenetic determinants of erythropoiesis: role of the histone methyltransferase SetD8 in promoting erythroid cell maturation and survival. *Mol. Cell. Biol.*, **35**, 2073–2087.

63. Zwifelhofer,N.M., Cai,X., Liao,R., Mao,B., Conn,D.J., Mehta,C., Keles,S., Xia,Y. and Bresnick,E.H. (2020) GATA factor-regulated solute carrier ensemble reveals a nucleoside transporter-dependent differentiation mechanism. *PLos Genet.*, **16**, e1009286.

64. Li,K., Miller,C., Hegde,S. and Wojchowski,D. (2003) Roles for an Epo receptor Tyr-343 Stat5 pathway in proliferative co-signaling with kit. *J. Biol. Chem.*, **278**, 40702–40709.

65. Munugalavadla,V., Dore,L.C., Tan,B.L., Hong,L., Vishnu,M., Weiss,M.J. and Kapur,R. (2005) Repression of c-kit and its downstream substrates by GATA-1 inhibits cell proliferation during erythroid maturation. *Mol. Cell. Biol.*, **25**, 6747–6759.

66. Jing,H., Vakoc,C.R., Ying,L., Mandat,S., Wang,H., Zheng,X. and Blobel,G.A. (2008) Exchange of GATA factors mediates transitions in looped chromatin organization at a developmentally regulated gene locus. *Mol. Cell*, **29**, 232–242.

67. Paralkar,V.R., Mishra,T., Luan,J., Yao,Y., Kossenkov,A.V., Anderson,S.M., Dunagin,M., Pimkin,M., Gore,M., Sun,D. *et al.* (2014) Lineage and species-specific long noncoding RNAs during erythro-megakaryocytic development. *Blood*, **123**, 1927–1937.

68. Hu,W., Yuan,B., Flygare,J. and Lodish,H.F. (2011) Long noncoding RNA-mediated anti-apoptotic activity in murine erythroid terminal differentiation. *Genes Dev.*, **25**, 2573–2578.